

Review

Plasmonic Nanosensors: Design, Fabrication, and Applications in Biomedicine

Valeria Nocerino ^{1,2,†}, Bruno Miranda ^{1,3,†} , Chiara Tramontano ^{1,4}, Giovanna Chianese ¹ , Principia Dardano ¹ ,
Ilaria Rea ^{1,*}  and Luca De Stefano ¹ 

¹ Institute of Applied Sciences and Intelligent Systems—Unit of Naples, National Research Council, Via Pietro Castellino 111, 80131 Naples, Italy; valeria.nocerino@na.isasi.cnr.it (V.N.); bruno.miranda@na.isasi.cnr.it (B.M.); chiara.tramontano@na.isasi.cnr.it (C.T.); giovanna.chianese@na.isasi.cnr.it (G.C.); principia.dardano@na.isasi.cnr.it (P.D.); luca.destefano@na.isasi.cnr.it (L.D.S.)

² Department of Engineering, Università degli Studi di Napoli Parthenope, Centro Direzionale di Napoli, Isola C4, 80143 Naples, Italy

³ Department of Electrical Engineering and Information Technology, Università Degli Studi di Napoli Federico II, Via Claudio 21, 80125 Naples, Italy

⁴ Department of Pharmacy, Università Degli Studi di Napoli Federico II, Via Domenico Montesano 49, 80131 Naples, Italy

* Correspondence: ilaria.rea@na.isasi.cnr.it

† These authors contributed equally to this work.

Abstract: Current advances in the fabrication of smart nanomaterials and nanostructured surfaces find wide usage in the biomedical field. In this context, nanosensors based on localized surface plasmon resonance exhibit unprecedented optical features that can be exploited to reduce the costs, analytic times, and need for expensive lab equipment. Moreover, they are promising for the design of nanoplatforms with multiple functionalities (e.g., multiplexed detection) with large integration within microelectronics and microfluidics. In this review, we summarize the most recent design strategies, fabrication approaches, and bio-applications of plasmonic nanoparticles (NPs) arranged in colloids, nanoarrays, and nanocomposites. After a brief introduction on the physical principles behind plasmonic nanostructures both as inherent optical detection and as nanoantennas for external signal amplification, we classify the proposed examples in colloid-based devices when plasmonic NPs operate in solution, nanoarrays when they are assembled or fabricated on rigid substrates, and nanocomposites when they are assembled within flexible/polymeric substrates. We highlight the main biomedical applications of the proposed devices and offer a general overview of the main strengths and limitations of the currently available plasmonic nanodevices.

Keywords: localized surface plasmon resonance; plasmonic nanoparticles; metal-enhanced fluorescence; surface-enhanced Raman scattering; optical biosensors; bioimaging; drug monitoring; colloidal nanoparticles; nanoarrays; nanocomposites



Citation: Nocerino, V.; Miranda, B.; Tramontano, C.; Chianese, G.; Dardano, P.; Rea, I.; De Stefano, L. Plasmonic Nanosensors: Design, Fabrication, and Applications in Biomedicine. *Chemosensors* **2022**, *10*, 150. <https://doi.org/10.3390/chemosensors10050150>

Academic Editor: Xiaobing Zhang

Received: 23 March 2022

Accepted: 18 April 2022

Published: 20 April 2022

Publisher's Note: MDPI stays neutral with regard to jurisdictional claims in published maps and institutional affiliations.



Copyright: © 2022 by the authors. Licensee MDPI, Basel, Switzerland. This article is an open access article distributed under the terms and conditions of the Creative Commons Attribution (CC BY) license (<https://creativecommons.org/licenses/by/4.0/>).

1. Introduction

In recent years, great advances in nanotechnology have largely found applications in the field of biomedicine. In this context, the optical properties of metallic nanomaterials such as gold (Au) and silver (Ag) nanoparticles (NPs) have been exploited to produce nano-diagnostic and nano-therapeutic smart systems, which are simple, exhibit fast response times, and are relatively low-cost [1–6]. Physics, engineering, chemistry, and material science have been combined with biology, biotechnology, and medicine to produce biomedical devices that convert biological and/or biochemical signals into electrical ones through electrical, optical, electrochemical, or piezoelectric transducers [7–11]. Nanomaterial-based transducers are finding large interest by the scientific community due to the peculiar physicochemical, optical, and electrical properties arising when their bulk counterparts are

reduced at the nanoscale [12]. Among the many available transducers based on nanotechnologies, optical nanobiosensors based on noble-metal NPs have shown great advances, becoming a leading technology with always improved sensing performances and smart applications [13]. Metal NPs can be used as optical transducers based on a phenomenon known as localized surface plasmon resonance (LSPR), which is the oscillation of the electron density on the surface of the NPs occurring at a specific excitation wavelength. A strong enhancement of the electromagnetic field occurs just in the surroundings of the NPs at a subwavelength level [14]. Therefore, when a metal nanoparticle interacts with an electromagnetic wave (i.e., light source), localized resonances are generated whose spectral positions are strongly affected by the shape, composition, and size of the particle [15,16]. The strong field enhancement in the surroundings of the plasmonic NPs confer to them high sensitivity to tiny refractive index (RI) variations in the proximity of the NPs [17]. Plasmonic NPs are converted into optical biochemical transducers when properly functionalized by a biorecognition element. The interaction between the biorecognition element and the target analyte generates a variation of the RI around the nanoparticles and thus a shift in the resonance frequency, which can be correlated to the concentration of the analyte of interest [18]. The LSPR phenomenon has been mathematically explained by Mie, who formulated his theory to explain the absorption and scattering cross-sections exhibited by very small colloidal particles (typically less than 100 nm) suspended in water [19]. Mie's theory provides the expression of the extinction as a function of the shape, size, and RI in the nanoparticle's surroundings [20]:

$$E(\lambda) = \frac{24\pi N_A a^3 \varepsilon_m^{\frac{3}{2}}}{\lambda \ln 10} \left| \frac{\varepsilon_i}{(\varepsilon_r + \chi \varepsilon_m)^2 + \varepsilon_i^2} \right| \quad (1)$$

In Equation (1), a is the radius of the nanoparticle, N_A is its real density, ε_m is the dielectric permittivity of the medium in which the NPs are immersed, λ is the excitation wavelength, ε_r and ε_i are the real and the imaginary part of the dielectric function of the nanostructure, respectively, while χ is used to describe the aspect ratio of the nanostructure. Starting from this relatively simple description of the basic phenomenon, researchers extended and applied this theory to more sophisticated systems with applications spanning from chemistry to optics, from biology to medicine.

A very simple colorimetric biosensor can be obtained from a colloidal suspension of nanoparticles, which assumes a typical coloration depending on the composition, size, and shape of the plasmonic NPs involved [21,22]. It is possible to induce their chemical aggregation by functionalizing them by a biorecognition layer, which can be sensitive to salts, pH, and target biomolecules. A deep colorimetric variation can be observed by the naked eye, leading to rapid and low-cost assays, which have been and are still extensively used for diagnostic purposes [23,24].

Moreover, as mentioned above, metallic NPs can be used as optical transducers by exploiting the intrinsic LSPR signal, which undergoes a red-shift or a blue-shift as a function of the RI increase or decrease in the proximity of the NPs. For example, when a biological analyte binds to the surface of an NP, a change of the RI (Δn) occurs, and therefore a frequency shift of the LSPR peak is observed. This behavior is described by the formula [20,25]:

$$\Delta\lambda = m(\Delta n) \left[1 - \exp\left(\frac{-2d}{l_d}\right) \right] \quad (2)$$

where m is the refractive index sensitivity, d is the thickness of the biorecognition layer, and l_d is the characteristic electromagnetic field decay length. Therefore, it is possible to use the plasmonic NPs immobilized on a substrate as refractometric transducers. LSPR measurements can be made in transmission, reflection, dark-field scattering, and total internal reflection.

Despite the intrinsic LSPR signal monitoring, plasmonic NPs have found large interest as antennas involved in the amplification of external signals arising from light-matter in-

teraction, i.e., Raman scattering, and fluorescence with applications in (bio)chemical assays. More precisely, surface-enhanced Raman scattering (SERS) [26,27] and metal-enhanced fluorescence (MEF) [28–30] sensing mechanisms are the object of many research studies. In SERS spectroscopy, the weak Raman signals typical of biomolecules (fingerprint recognition) can be enormously amplified (up to 10 orders of magnitude) by placing the target in the proximity of plasmonic NPs. The Raman signal amplification by metallic nanoparticles is generally attributed to two main contributions: electromagnetic enhancement and chemical enhancement [31,32]. The experimental evaluation of the average Enhancement Factor (EF_{SERS}) can be performed by applying the following formula:

$$EF_{SERS} = \frac{I_{SERS}}{I_{Raman}} \frac{N_{Raman}}{N_{SERS}} \quad (3)$$

where I_{SERS} and I_{Raman} stand for the intensities of Raman and SERS signals, respectively, and N_{SERS} and N_{Raman} are the average number of molecules in the scattering volume in each measurement [33]. Differently, metal-enhanced fluorescence induced by plasmonic nanoparticles is still not fully understood, but it strongly depends on (i) the spectral overlap between the plasmon extinction and the excitation (Förster resonance energy transfer (FRET) mechanism) and/or emission (Purcell mechanism) of a fluorescent dye, and (ii) on the distance between the fluorophore/NP couple [34–36].

Nanobiosensors using plasmonic NP-based optical transducers can be made in solution (colloids), or by depositing metal nanoparticles on dielectric substrates, creating periodic or non-periodic arrays, or by deposition/embedding on/into polymeric materials. Several protocols for the fabrication of metal nanoparticles of different shapes and sizes have been published; the most used synthesis methods are electron beam lithography (EBL), colloidal assembly, and nanosphere lithography. The most widely used bottom-up synthesis method is the colloidal assembly in which a solution of metallic salts is reduced via chemical agents, such as sodium citrate, which confers a negative charge to plasmonic NPs. Then, the NP surface can still be modified with stabilizing molecules (thiolate), or even polymeric ligands, which are essential to avoid NP aggregation and ensure their colloidal stability [37]. Plasmonic nanoarrays can be fabricated on a large scale by using top-down, bottom-up, or mixed fabrication strategies [34,38–40]. The tailoring of the optical properties of plasmonic arrays can be engineered according to the desired applications by changing the size, shape, material, and distance of plasmonic NPs. Finally, polymeric nanocomposites can be obtained by three main mechanisms: deposition of colloidal NPs onto polymeric substrates, preparation of a pre-polymer solution embedding plasmonic NPs followed by curing (i.e., polymerization, curing, electrospinning), and in-situ reduction of plasmonic NPs on/within a polymeric matrix [3,41].

In this review, we summarize the most recent plasmonic nanobiosensors proposed for applications in biomedicine by considering the main fabrication techniques related to colloids, arrays, and flexible plasmonic substrates. Particular attention is given to their application in both inherent resonance-based biosensors and signal amplification-based biosensors. We describe the chemical mechanisms involved in both label-free and non-label-free sensing mechanisms, the achieved limits of detection, and their application in the biomedical field. Finally, we provide an overview on the main advances in the integration of plasmonic transducers within point-of-care (POC) testing devices by combination with microelectronics and microfluidics to achieve ultra-compact, low-cost, and easy-to-use platforms for applications in biomedicine without the need of expert personnel.

2. Plasmonic Colloids for Biomedicine

2.1. LSPR-Based Colorimetric Biosensors

The composition, size, and shape of plasmonic NPs are all parameters that strongly affect their LSPR response and introduce themselves as excellent optical transducers for the development of innovative sensors [16]. The interaction between the recognition element and the analyte of interest results in a shift of the LSPR related to the concentration of the

analyte of interest. The recognition element is responsible for the specificity and selectivity of the sensor. In recent years, the real challenge was to produce simple and low-cost diagnostic devices able to show results in a short time [42]. In this context, colorimetric sensors, providing a visible response to the naked eye, turned out to be excellent candidates. In this section, colorimetric sensors for different applications are presented. Size and shape, the limit of detection (LOD), and the selectivity of the NPs are detailed. It is well known that the LSPR spectral shape and the wavelength of the peak maximum depend on the material, the size, and the shape of the NPs [43,44]. The material is the crucial choice in the development of the sensor. Gold is preferred to obtain a platform with high chemical stability and resistance to oxidation, whereas silver is used to have sharper resonances and higher sensitivity to refractive index variations [14,45]. For example, gold NPs of 50–60 nm in diameter have a plasmon resonance at 530 nm and a refractive index sensitivity of 60 nm/RIU, while silver NPs of 50–60 nm have a plasmon resonance at 435 nm and a refractive index sensitivity of 160 nm/RIU [45,46]. Shape is also an important parameter to evaluate; 20 nm spherical gold NPs have an LSPR at a wavelength of 520 nm, whereas gold nanorods of 10–20 nm in diameter and 10–100 nm in length show two plasmonic bands at 520 nm and 700 nm due to the longitudinal and transverse resonance, respectively; in addition, gold nanocubes of 44 nm in size have an LSPR peak at 538 nm and a sensitivity of 83 nm/RIU, whereas silver nanocubes of 30 nm in size have an LSPR peak at 510 nm with a high sensitivity of 146 nm/RIU [44,47–49] (Figure 1a). Over the years, LSPR-based sensors with nanoparticles of different shapes or sizes for the detection of a large variety of molecules involved in diagnostics have been proposed. The relevance of LSPR sensing in nanomedicine was also demonstrated in early stages of cancer diagnosis [50] (Figure 1b). The detection of specific prostatic antigen (PSA) was performed through 10 nm-gold particles covalently bound to the anti-PSA monoclonal antibody [51]. Parameters such as pH, temperature, and concentration *ratio* between the gold NPs and the anti-PSA were optimized to facilitate the covalent bond. The presence of the anti-PSA generated a 28 nm-redshift in the gold absorption peak from 510 nm, confirming the immobilization of the antibodies on NPs, and the presence of the analyte PSA in the test sample caused a further redshift (up to 578 nm). The LOD, in this case, was 0.2 ng/mL, and the selectivity was assessed with two different tumor markers, generating no spectral change. Velotta et al. proposed a colorimetric sensor to detect the presence of human immunoglobulin G (IgG) in simulated fluids (Figure 1c) [23]. In this work, 40-nm gold NPs, synthesized and stabilized with sodium citrate, were used to immobilize the antibody by the photochemical immobilization technique (PIT) [52,53]. The presence of the analyte of interest caused an aggregation process of the colloidal solution in combination with an increase in the average size of the NPs. Therefore, a redshift of the plasmon of about 3.4 nm from the peak of LSPR of gold NPs at 540 nm is visible both to the naked eye and via spectrophotometric analysis. Despite the LOD of the sensor being just 100 ng/mL, the rapid response and the practical use make the sensor an efficient tool for mass screening. To develop sensors with better performances, researchers also used a combination of different noble metals such as gold and silver. In this regard, Di et al. developed a coupled system built on gold/silver NPs for the colorimetric detection of glucose (Figure 1d) [54]. In this case, gold NPs were used as a catalyzer to oxidate glucose, and silver NPs acted as an alternative to chromogenic agents for detecting glucose. Briefly, gold and silver NPs were synthesized by using sodium citrate as both reducing agent and stabilizer, and their dimensions were about 4 nm and 10.8 nm, respectively. When glucose was added to a buffer solution containing gold NPs, they catalyzed the oxidation of the glucose and produced H₂O₂, which caused dissolution of the silver NPs, inducing a change in the plasmon resonance. This change was visible to the naked eye, since the solution color shifted from yellow to red. Therefore, it was possible to determine the presence of glucose in a quicker and lower-cost way with an LOD of 3 μM.

In another study for glucose monitoring, the properties of a small amphiphilic protein (Vmh2) were exploited: it could spontaneously interact with glucose [55]. In this work, 8 nm gold NPs were synthesized with polyethylene glycol (PEG), and the obtained

solution appeared in a shade of red and pink [56]. The NPs were functionalized with hydrophobins (HFB), and the solution changed color from red/pink to purple [57]. The HFB-functionalized NPs were mixed with glucose at different concentrations, and the variation of the gold LSPR was monitored by spectrophotometry. The main purpose of this work was to produce hybrid NPs to improve biocompatibility. The experimental results were obtained through UV–Vis spectroscopy, dynamic light scattering measurements, polarization modulation–infrared reflection–adsorption spectroscopy (PM-IRRAS), and X-ray photoelectron spectroscopy (XPS).

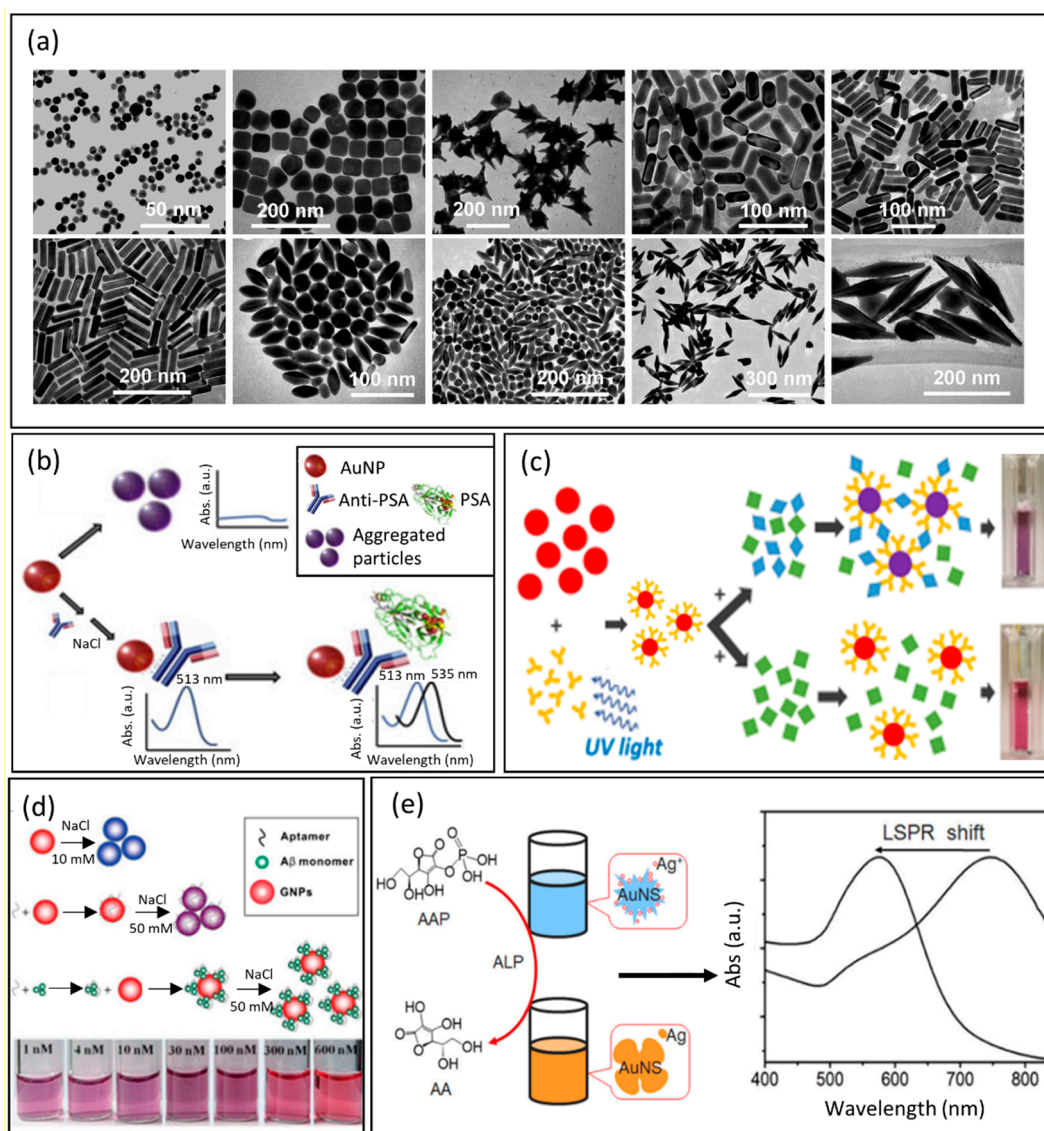


Figure 1. (a) From left to right, representative TEM images of Au nanoparticles of different shapes: on the top, nanospheres, nanocubes, nanobranched, nanorods (aspect ratio = 2.4 ± 0.3), and nanorods (aspect ratio = 3.4 ± 0.5); on the bottom, nanorods (aspect ratio = 4.6 ± 0.8), nanobipyramids (aspect ratio = 1.5 ± 0.3), nanobipyramids (aspect ratio = 2.7 ± 0.2), nanobipyramids (aspect ratio = 3.9 ± 0.2), and nanobipyramids (aspect ratio = 4.7 ± 0.2). Reproduced Adapted with permission from Ref. [48]. Copyright (2008), American Chemical Society. (b) Representation of the mechanism of the optical nanosensor for the detection of PSA. Colloidal AuNPs change color from red to purple in the absence of antibody proteins. The conjugation of antibodies to AuNPs stabilizes them and enables the detection of PSA. Adapted with permission from Ref. [50]. Copyright (2021), Elsevier. (c) Colorimetric

detection scheme. AuNPs are functionalized with Abs by the photochemical immobilization technique (PIT), and then the presence of specific antigen induces the colorimetric variation of the colloidal solution from red to purple. In this case, there is the controlled aggregation of nanoparticles. Adapted with permission from Ref. [23]. Copyright (2018), American Chemical Society. (d) Detection of DNA-aptamer based on the colloidal solution of gold nanoparticles. Adapted with permission from Ref. [58], Copyright (2018), MDPI-open access article under the Creative Commons Attribution License. (e) Schematic representation of colorimetric detection of ALP. The blue shift of LSPR depends on the amount of enzyme that reduces silver nanoparticles on the surface of AuNSs. Adapted with permission from Ref. [59]. Copyright (2016), Elsevier.

The flexibility to modify the surface of NPs has also made LSPR-based nanosensors very for the detection of bacteria. Nemati's group developed an immunodiagnostic sensor able to detect the presence of *V. cholerae* O₁, a gram-negative bacterium involved in cholera disease [60]. In this work, the synthesis of gold NPs with a size of 40 nm was performed using trisodium citrate, and their surface was functionalized by a monoclonal antibody able to recognize bacteria [58]. Monitoring the LSPR shift, it was possible to evaluate the concentrations of *V. cholerae* down to an LOD of 10 CFU/mL. A different strategy for biosensing through enzyme-guided growth of silver NPs on gold nanostars was reported by Ju et al. [59]. Once again, they combined the properties of gold and silver to obtain better performances. Alkaline phosphatase (ALP), in presence of ascorbic acid 2-phosphate (AAP), produced a reductant acting on the silver NPs available on the 55 nm gold nanostars (AuNSs). The reduction of the silver NPs (AgNPs) resulted in a blue shift of the LSPR and a change of the AuNSs' color from blue to purple, and then to orange. According to this, it was possible to quantify the amount of enzyme that reduced the silver NPs on the surface of the AuNSs (Figure 1d). The biosensor LOD was 0.5 pM, and it is well to underline that this method can be easily combined to detect other biomolecules by the naked eye. Since the surrounding of the NPs affects the LSPR, and the LSPR peak wavelength shift is proportional to the changes in the refractive index of the surrounding, this property could be useful to estimate the thickness of a biopolymer wrapping NPs, as proposed by Tramontano et al. [61]. The authors monitored the gelatin thickness on the surface of diatomite NPs due to the AuNPs grown in situ on their surface. The formation of a gelatin shell around the NPs resulted in a change of the refractive index and a redshift proportional to the thickness of the gelatin. Moreover, when enzymes or other conditions degraded the gelatin shells, a blue shift occurred, and it could be related to the released drug. In recent years, the COVID-19 pandemic has increased the request of assays with results easily interpretable by naked-eye or by a simple UV-Vis spectrometer. In this context, various LSPR biosensors have been presented [22,62–64], among which Liv et al. realized a colorimetric biosensor to detect the presence of the SARS-CoV-2 spike antigen [65]. In this study, 15 nm gold NPs (AuNPs) were synthesized by the standard citrate reduction method, and then the citrate groups were displaced by 11-mercaptoundecanoic acid (MUA). The SARS-CoV-2 spike antibody (Mab) was covalently bound to the NPs. After functionalization, the AuNPs appeared dimensionally larger (34 nm), and the LSPR peak redshifted to 526 nm. In the presence of the SARS-CoV-2 spike antigen, the LSPR peak underwent a further redshift of about 25 nm, detectable by the naked eye, since the color of the colloidal solution quickly shifted from red to purple. In this case, the LOD was 48 ng/mL, and the selectivity was demonstrated using two different spike antigens. A summary of the reported LSPR-based colorimetric biosensors is provided in Table 1.

Table 1. Examples of LSPR-based colorimetric biosensors.

Material	Shape	Size (nm)	Analyte	Linear Range	Sensitivity	LOD	Ref.
Gold	Spherical	9	PSA	0.2–1 ng/mL	43.75 nm/(ng mL ⁻¹)	0.2 ng/mL	[50]
Gold/Silver	Spherical	4	Glucose	5–70 μM		3 μM	[54]
Gold	Spherical	8 ± 3	Glucose	0.3–1.2 mg/mL	0.13 ± 0.06 a.u./(mg mL ⁻¹)	7.3 ± 0.3 mg/mL	[55]
Gold	Spherical	43	<i>V. cholerae</i> O1	10–10 ⁴ CFU/mL		10 CFU/mL	[60]
Gold/Silver	Nanostars	55 ± 5	Alkaline phosphatase (ALP)	1.0 pM to 25 nM		0.5 pM	[59]
Gold	Spike-like nanoparticles		Hemagglutinin	1 pM to 10 nM		1 pM	[62]
Gold	Spherical	55 ± 5	SARS-CoV-2 viral RNA	0.2–3 ng/μL		0.18 ng/μL	[64]
Gold	Spherical	16	SARS-CoV-2 spike antigen		0–1000 ng/mL	48 ng/mL	[65]

2.2. SERS-Based Colloidal Sensors for Bioimaging and Biomedical Applications

The direct analysis of biological processes and functions is crucial for understanding both physiological cell activity and pathological abnormalities. The direct study of living cells, tissues, or organs through in situ non-invasive methodologies is necessary for understanding the complexity of the processes underlying diseases, and testing strategies for clinical treatment. The modern analytical techniques (fluorescence [66], chromatography [67], spectroscopy [68]) used in biomedicine show ultrahigh sensitivity and high-performance levels for imaging, drug release monitoring, cell mapping [69], and other medical purposes. However, they have certain inevitable limitations. For instance, when it comes to tracking molecules or NPs inside cells, the most implemented approach is based on fluorescence [70]. This approach requires labeling the molecule with fluorophores or dyes that might affect the pharmacological effect of the drug. Moreover, fluorescence is sensible to photobleaching, causing under or over-estimation in the sample quantification.

Other strategies employed in disease diagnosis, pathogenic environmental monitoring, and healthcare screening are expensive and require extensive manipulation of the sample before analysis, hindering the real-time investigation of biological processes. In the request for rapid and non-destructive platforms for biomedical purposes, SERS-active platforms optimally adapted in shape have been demonstrated to complement traditional approaches, offering real-time in vitro and in vivo analyses [71]. SERS arises from the coherent oscillation of the electrons in noble metals and the excitation of LSPRs at specific wavelengths of incident light. When a molecule is adsorbed at the hot spot, the excitation and Raman field are both enhanced, giving rise to a giant amplification of the scattering signal up to 10¹⁰ [72]. Since most of the chemical and biological compounds have unique Raman fingerprint patterns, SERS enables sensitive and label-free investigations of a wide array of interesting analytes. Noble metal particles, such as gold (Au) or silver (Ag) in suspensions or immobilized on a substrate [73], are by far the most used substrates, since their LSPR response can be easily excited producing enhancement on the order of 10³–10⁴ [74]. Managò et al. showed that gold-decorated silica NPs can be used as a SERS platform for monitoring and quantifying the amount of Galunisertib released in living colorectal cancer (CRC) cells without needing external fluorophores or markers [75]. In this work, the AuNPs grown on the surface of DNPs by an in-situ approach produced an enhancement of the Raman drug signal of 10⁵ and allowed a quantification down to a sub-femtogram scale resolution. The author reconstructed a false Raman map (Figure 2a) to study the internalization of the hybrid delivery system. Then, thanks to the strong Raman drug enhancement provided by AuNPs, the drug release was monitored at different time intervals in vitro (Figure 2b) and CRC cells (Figure 2c), making it easy to correlate the amount of released drug to the observed biological outcome. In this study, SERS represented a precise and rapid tool

to understand the release behavior of the drug delivery system in the cell, overcoming traditional spectroscopic or fluorescent issues for drug monitoring [68]. The possibility to analyze samples using a fast, sensitive, and non-destructive method is thus fundamental when handling sensitive samples such as cells during *in vitro* investigations. For instance, the cell uptake of NPs can be monitored by different techniques, including TEM [76], but most of them can damage cells or allow for analysis of only a small portion of the cell volume. SERS, instead, can be used as an excellent tool for the study of the NPs' cell uptake and their mechanism of internalization. The main advantage of using SERS rather than TEM relies on the time and costs required for the analysis. Kapara et al. functionalized AuNPs with an anti-ER α (Estrogen Receptor-alpha) antibody and a Raman reporter to investigate the internalization and localization of ER α -AuNPs in breast cancer cells [77]. ER α -AuNPs were incubated with cells for a shorter time and without the use of fluorescent staining, which needs expensive primary and secondary antibodies. The authors realized 3D SERS images of the entire cell volume and showed that modified AuNPs cannot penetrate breast cancer cells by passive targeting, but with a receptor-mediated pathway driven by their binding to the ER α receptor in the plasma membrane. The internalization of AuNPs is a crucial factor determining their application in nanomedicine, and the possibility to investigate their cell uptake with non-invasive techniques is mandatory to discriminate between the toxicity caused by either AuNPs or the technique. The safety of AuNPs, such as any material for human use, needs accurate evaluation and reliable techniques as well. SERS found application also in the detection of toxic contaminants (bacteria, endotoxins, toxins, and viruses [26] in AuNPs, since this material can be contaminated by a bacterial endotoxin known as "liposaccharide", a potent cause of immunoreactivity in mammals [78]. The detection of LPS in AuNPs can be challenging because they can interfere with the most common assays (limulus amoebocyte lysate (LAL), monocyte activation test (MAT) [79]), altering the final readout of the analysis. Verde et al. showed that SERS can complement the traditional techniques to detect LPS directly on AuNPs with chemical specificity among different types of LPS or bacteria, such as *Escherichia coli* and *Klebsiella pneumoniae*. They developed a sensitive platform with a detection limit of 5 LPS molecules per AuNPs, high-reproducibility, and without modifying the AuNP surface through functionalization approaches [80]. Furthermore, the authors showed that AuNPs did not produce biologically significant toxic effects in macrophages and that most of the inflammatory response is driven by the presence of LPS. Therefore, this study supported the use of AuNPs as safe imaging material for biomedical applications and offered a reliable technique for assessing the absence of toxic LPS before using AuNPs in medicine. To obtain higher enhancement of the Raman scattering, noble metal films can be realized on three-dimensional (3D) SERS substrates that are promising platforms for the analysis of complex samples [81]. The 3D SERS substrates show excellent sensing performance, since they allow for 3D plasmonic coupling both in-plane and out-of-plane, expanding the hotspot of the 3D volume compared to the 2D substrates [82]. These 3D structures can be found in nature, such as insects, birds, and flowers, which possess periodic micro and nanostructures with efficient light manipulation and plasmonic properties [83]. In recent years, the dielectric nanoarchitecture of diatom shells served as low-cost platforms for SERS sensing of biological compounds [84]. Managò et al. showed that a silica/metal hybrid structure composed of diatom valve and Au can be applied for the chemical analysis of both red blood and leukemia cells thanks to a robust SERS amplification (EF) of 4.6×10^6 [33]. The metalized frustule was developed using Au thermal evaporation to grow a metal layer on the 3D silica nanoarchitecture. The main advantage of diatom-based SERS platforms is their low-cost production and 3D natural periodic and sub periodic architecture, which make them valid alternatives to costly and complex 3D geometries [85]. Indeed, the metalized frustule offered the possibility to analyze the cell membrane thanks to the unique cell spectral signature from Raman scattering, supporting the use of SERS for the detection of several oncological disorders. In recent years, there has been an increasing number of publications reporting the employment of SERS for *in vivo* investigations, especially for

cancer imaging and detection [86]. SERS-encoded particles (SEP) made of a plasmonic NP core (silver or Au) coated with a SERS probe have shown a high photostability and optical contrast when working with cells and near-infrared (NIR) excitations [87].

SEP can be functionalized with a wide range of biological moieties [88–90] to promote the preferential accumulation of NPs in tumors compared to normal tissues. Nicolson et al. developed a SEP-based biosensor for visualizing the diffusion of brain main tumor and delimiting the margins, isolating distant tumor clusters of fewer than five cells in vivo [91]. The author synthesized Au nanostars (AuNSs) coated by silica and further functionalized with a SERS probe and the tripeptide RGD (arginyl glycylic aspartic acid) for targeting integrin, which is predominantly expressed on tumor endothelial cells (Figure 2d). To avoid background interference with the Raman signatures of interest, the authors combined spatially offset Raman spectroscopy (SORS) with the SERS technique, making it possible to obtain excellent tumor localization with a power density five times less than that used for conventional Raman spectroscopy. Thanks to their unique Raman fingerprint, RGD-AuNPs allowed for the identification of metastasis located at about 350 μm from the main tumor by Raman imaging. Integrin targeted RGD-AuNPs-SEP enabled an accurate outline of the brain tumor and localization of microscopic extensions invading the brain, in agreement with the magnetic resonance imaging (MRI) (Figure 2e,f). It was also possible to detect isolated glioblastoma cells on their migratory path. These results, among others reported in the literature and this section, hold promise to allow high precision visualization and mapping of tumors [92] and the extents of metastasis. The attention that SERS has gained in the last decade for in vitro/vivo applications is supported by the opportunity to overcome limitations held by traditional techniques that are time-consuming, costly, and not as sensitive and accurate as SERS for performing real-time analysis in complex samples.

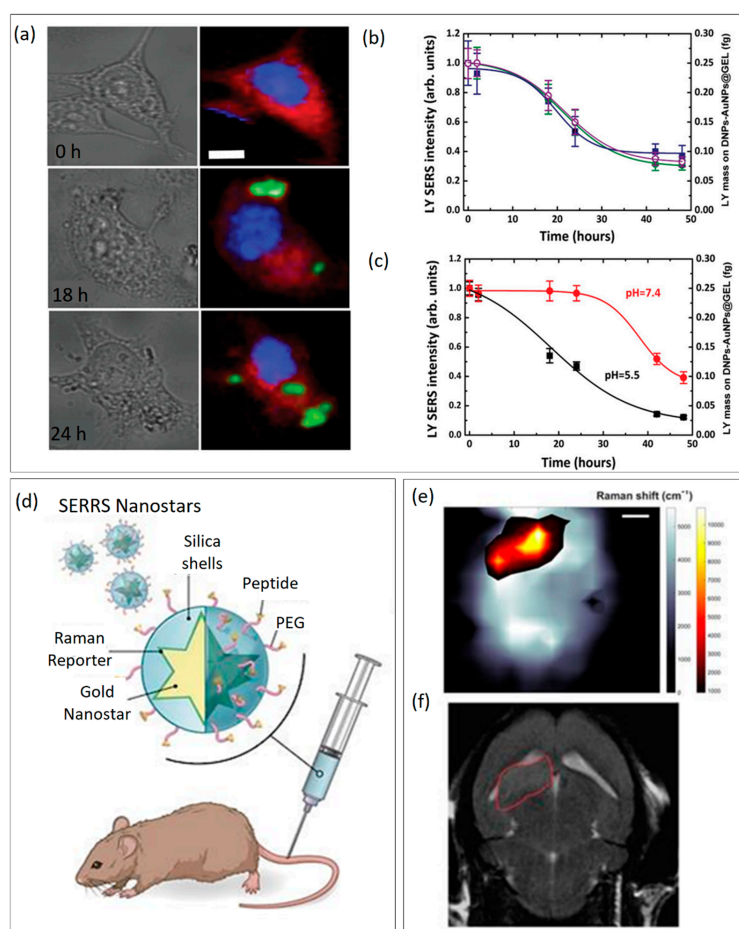


Figure 2. (a) False map reconstructed by Raman imaging through the MCH approach for analyzing

the internalization of hybrid DNPs in cells. (b) Drug release studies monitored in CRC cells by real-time SERS. (c) Drug release studies monitored in phosphate buffered saline (PBS) pH 7.4 and 5.5 by real-time SERS. Adapted with permission from Ref. [75]. Copyright (2021), John Wiley & Sons. (d) Functionalization of active-targeted nanostars for in vivo imaging of brain tumors. (e) The SORS heat map confirming the presence of a brain tumor is in good agreement with the MRI image (f). Adapted with permission from Ref. [91]. Copyright (2019), Ivyspring International Publisher.

3. Plasmonic Nanoarrays for Biomedicine

One of the best ways to improve the LSPR sensors' performances is to enhance the interactions between light and matter. In this regard, in addition to the growing development of colorimetric sensors, based on solution assays, new nanotechnologies have been developed that can effectively improve the light–matter interaction [93]. Although the potentiality of colloidal plasmonic NPs has been elucidated, with a particular focus on their application in biosensing and bioimaging applications, some of the major issues associated with them are the chemical stability and signal reproducibility, which could hinder their application at the industrial level [94–96]. Moreover, the quest for easy-to-read, rapid, and portable devices has pushed scientists towards the design of optical substrates based on plasmonic NPs, whose response could be easily monitored by simple spectroscopy. Several techniques have been proposed to produce plasmonic periodic, quasi-periodic, and non-periodic nanoarrays with precise optical properties, which could be exploited for biochemical sensing and whose performance strongly depended on the size, shape, material, and interparticle distance of the proposed nanoplatform [97]. Three methods are generally recognized for the fabrication of plasmonic nanoarrays: top-down, bottom-up, and mixed approaches [38,40,98–100]. The first one is generally the most expensive and time-consuming and leads to the fabrication of periodic nanoarrays with an easily predictable and tunable optical response. “Hard” lithography (e.g., E-beam lithography) is generally employed for this type of approach, providing arrays with always renewed optical performance, which can be exploited in biomedicine to achieve ultra-low limits of detection and extremely high sensitivities [101]. Vice versa, the bottom-up approach promises low-cost and large-scale substrates starting from chemically synthesized plasmonic NPs, which are self-assembled on an optically transparent or reflecting substrate. This technique does not require expensive instruments and offers the opportunity to have access to plasmonic arrays, which are generally non-periodic or quasi-periodic, and which exhibit reduced analytical performance in the biosensing field but could be in principle applied on a large scale. Generally, plasmonic nanoarrays assembled via this technique show great potential in external signal applications for MEF and SERS-based biosensors [88]. Finally, a mixed fabrication approach takes advantage of the two previously mentioned fabrication approaches and offers a good trade-off between large-scale fabrication, costs, and performance [34]. In this section, we summarize the most recent plasmonic nanoarrays for intrinsic LSPR sensing and external signal amplification (SERS and MEF). Plasmonic nanoarrays can be engineered starting from structural parameters and generally exhibit better performance, better reproducibility, and multi-target detection compared to colloidal nanoparticles [102].

3.1. LSPR-Based Plasmonic Nanoarrays

The worldwide recognition of the main applications of plasmonic nanoarrays exploits the shift of the LSPR exhibited by noble-metal nanoparticles upon changes in the refractive index (RI) of the surrounding environment for bulk refractive index sensing and biochemical sensing [14]. This means that when properly functionalized with a biorecognition element, plasmonic NP absorption peaks undergo a redshift, which is generally proportional to the concentration of the used bioprobe. Unlike colloidal NPs, whose red-shift is generally due to NP aggregation, which can be monitored by the naked eye, when dealing with plasmonic nanoarrays, the tiny red-shifts measured by spectroscopic techniques are only due to the variation of the surrounding refractive index. The sensitivity (S) of

a plasmonic nanoarray is a parameter that describes its intrinsic capability of undergoing a redshift upon variation of the refractive index in the proximity of the plasmonic nanoarray surface:

$$S = \frac{d\lambda}{dn} \quad (4)$$

S is measured in nm per refractive index unit (nm/RIU). This parameter is not sufficient to describe the overall sensing capabilities of an LSPR-based optical transducer. Given the full width at half maximum ($FWHM$) parameter to describe the sharpness/broadness of the plasmon resonance, it is possible to introduce the figure of merit (FOM) as

$$FOM = \frac{S}{FWHM} \quad (5)$$

This parameter describes the performance of an LSPR-based optical transducer. More generally, in the biosensing community, gold is generally preferred to silver due to its chemical stability. However, silver exhibits sharper resonances, which boost the FOM of silver-based plasmonic nanoarrays. The oxidative susceptibility of silver hinders its application in LSPR-based biosensors; however, several strategies have been implemented to protect it from chemical oxidation [103,104]. The applications of LSPR-based plasmonic devices, in the diagnostic field, can be manifold. As an example, the detection and quantification of IgG can be a reliable means for the determination of some diagnoses such as hepatitis B virus, renal failure, hyperstimulation of the immune system, and some types of cancer [105]. Moreover, IgG could be used as biorecognition elements for biomarkers, cells, viruses, as well as pesticides and pollutants.

Both periodic and non-periodic plasmonic nanoarrays have been proposed for IgG-based sensing. Vestri et al. recently proposed a plasmonic 2D nanostructure based on a periodic arrangement of iso-Y gold NPs (Figure 3a). The array was fabricated by EBL lithography, its optical response was numerically evaluated, and a sensitivity of 412 nm/RIU was measured. The proposed platform was functionalized with IgG and allowed for the detection of a pesticide (namely, the imidacloprid) in the dynamic range of 1–1000 ng/mL achieving an LOD of 1 ng/mL [106]. Chen et al. proposed instead a multiplexed detection based on IgGs using large-scale plasmonic nanoarrays based on thermal dewetting of gold films of 10 nm thickness. They achieved a sensitivity of 104 nm/RIU and still a good LOD of multiple biomarkers, including IgG [107]. Another interesting application of LSPR-based plasmonic nanoarrays in the diagnostic field concerns the detection of cancer biomarkers, such as the prostate cancer-specific antigen (PSA). In [108], the specific binding between PSA-specific DNA aptamers and the LSPR optical response of gold nano-disks arrays on glass slides were exploited. DNA-aptamers were attached to the glass substrates with gold nano-disks, which before immobilization were first heated to 90° and then cooled to room temperature to maintain the flexibility of the aptamers, which was critical for PSA binding. Two different substrates were used to consider two different concentrations of aptamers. The binding between aptamer and gold nano-disks occurs between SH groups and Au atoms. The proposed platform exhibited a sensitivity of 113 nm/RIU and achieved an LOD of 1.49 ng/mL (Figure 3b). These results show the potentiality of plasmonic nanoarrays combined with aptamers, which could find large applications for pre-biopsy testing for cancer and partly avoid invasive exams [109]. Another example of PSA detection by plasmonic nanoarrays was achieved by using silver nano-columns [110]. The nano-columns with a diameter between 5 nm and 10 nm were immobilized on a glass substrate. They were stabilized by a self-assembled monolayer (SAM) of 11-mercaptoundecanoic acid (MUA) and 6-mercaptohexanol (MCH), and then the substrates were immersed in solutions containing different concentrations of anti-PSA. In this case, the achieved LOD was 850 pg/mL with clinically acceptable specificity, confirming the better performance of silver compared to gold when properly stabilized. Plasmonic nanoarrays can be therefore employed in the monitoring of the state of health and wellness of human beings. Recently, there have been numerous studies that have shown that vitamin D deficiency can be associated with

various diseases, even serious ones, such as cardiovascular disease and osteoporosis; on the other hand, an excess can lead to kidney failure [111]. Recently, a sensor based on bottom-up synthesized gold nanorods immobilized on a glass substrate was proposed for the detection of 25-hydroxyvitamin D₃, whose level in the blood can be directly traced back to that of vitamin D₃ [112]. The gold nanorods were synthesized directly with citrate, used as a stabilizer, and subsequently functionalized with an aptamer capable of binding specifically only with 25-hydroxyvitamin D₃ (Figure 3c). In this case, 1,6hexanedithiol was used as a blocking agent to promote specific binding, which improves LSPR and thus detection performance. This aptasensor showed a large dynamic range (0.1–105 ng/mL), which was considered clinically relevant to evaluate a deficiency or an excess of vitamin D. The achieved LOD was 0.1 ng/mL. A last interesting application of LSPR-based plasmonic nanoarrays concerns virus sensing. As an example, the hepatitis B virus (HBV), which is the culprit of hepatitis B disease, can lead to severe consequences as well as hepatocellular carcinoma (HCC) [113]. Gold NPs were synthesized using a gold nanoseed growth method, and then conjugation with the anti-HBsAg antibody on a glass substrate was performed [114]. The solution was later inoculated with the target analyte. To increase the sensitivity and enhance the optical response of the device, a second layer of AuNPs conjugated with anti-HbsAg was created to obtain a heteroassembled AuNP sandwich-immunoassay chip format. Three different sizes of gold nanoparticles were synthesized, namely 15 nm, 30 nm, and 50 nm, respectively, and using the 15 nm ones for both the first and second layer, a lower LOD of 100 fg/mL in 10–15 min was obtained. With a single layer of 15 nm AuNPs, the LOD was 10 pg/mL. One of the most recent applications of plasmonic nanoarrays is related to the COVID-19 pandemic outbreak, whose early diagnosis still represents the most powerful tool to prevent its spread. In this regard, a biosensor combining plasmonics and microfluidics-based on Au nanospikes fabricated by gold electrodeposition was proposed [115]. Optical sensing of anti-SARS-CoV-2 spike protein antibodies was performed in diluted human plasma without any labeling agents, reaching an LOD of 0.08 ng/mL, exhibiting complementing performances to the existing serological COVID-19 tests. Being based on a large-scale fabrication approach, the proposed platform could find application as a multiplexed biosensing platform for disease monitoring. Depending on the application and the desired performance, periodic as well as non-periodic structures of different shapes and sizes and materials can be fabricated and applied in the rapid diagnosis of diseases. A summary of LSPR-based plasmonic nanoarrays is provided in Table 2.

Table 2. Examples of LSPR-based plasmonic nanoarrays.

Material	Array Structure	Fabrication Method	Analyte	Linear Range	Sensitivity	LOD	Ref.
Gold	Periodic iso-Y NPs	EBL lithography	Imidacloprid	1–1000 ng/mL	412 nm/RIU	1 ng/mL	[106]
Gold	Single-layer four-channel microfluidic device	Physical vapor deposition + rapid thermal annealing	IgG and CRP		108.9 ± 1.3 nm/RIU		[107]
Gold	Nanodisk arrays	Deposition on glass slides	PSA	1.7–20.4 ng/mL	113 nm/RIU	1.49 ng/mL	[108]
Silver	Nano-columns	Glancing angle deposition	PSA	0.5–24 ng/mL	134 nm/RIU	850 pg/mL	[110]
Gold	Nanorods	Seed-mediated growth method	25-hydroxyvitamin D ₃	0.1–10 ⁵ ng/mL		0.1 ng/mL	[112]
Gold	Heteroassembled nanoparticles	Nanoseed growth on glass substrate	Hepatitis B virus			100 fg/mL	[113]
Gold	Nanospikes	Electrodeposition	Anti-SARS-CoV-2 spike protein antibodies		183 ± 10 nm/RIU	0.08 ng/mL	[115]

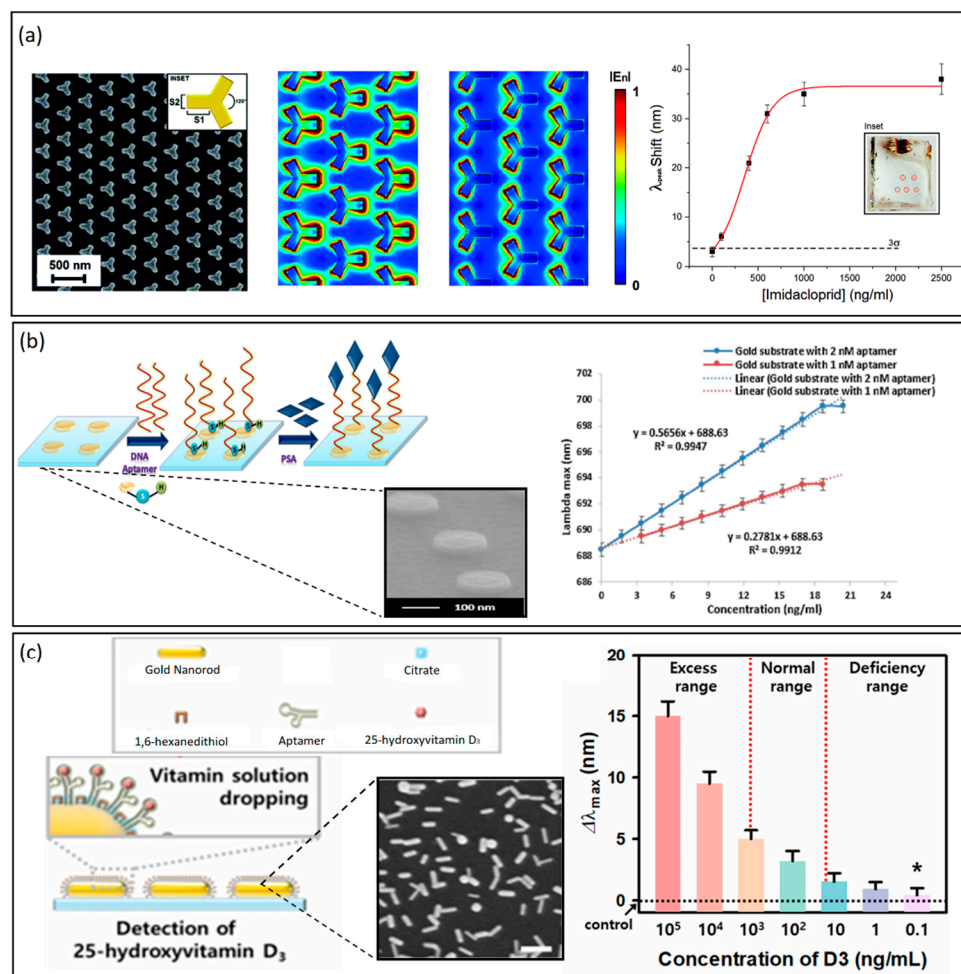


Figure 3. (a) From left to right: a plasmonic 2D nanostructure based on a periodic arrangement of iso-Y gold NPs, electric field enhancement simulations, and detection of imidacloprid pesticide achieving an LOD of 1 ng/mL. Adapted with permission from Ref. [106]. Copyright (2021), Royal Society of Chemistry. (b) From left to right: detection scheme of PSA through aptamers covalently bound to gold atoms. SEM image of gold nano-disks on a glass substrate. A linear relationship between λ_{max} shifts and the change of PSA concentration for two gold substrates having different concentrations of DNA aptamers. The dotted lines are the theoretical curves, while the continuous lines are the experimental curves. Adapted with permission from Ref. [108], Copyright (2018), Elsevier. (c) From left to right: detection scheme of 25-hydroxyvitamin D₃ by gold nanorods (AuNRs) immobilized on a glass substrate. SEM image of AuNRs. 25-Hydroxyvitamin D₃ detection by AuNRs based on λ_{max} shifts for a wide range of concentrations (0.1–105 ng/mL). Adapted with permission from Ref. [112], Copyright (2021), Elsevier.

3.2. Plasmonic Nanoarrays for MEF-and SERS-Based Biosensors

Nanostructured plasmonic arrays promise the advantage of being highly controllable, optically stable, and easy to tune via advanced photolithographic techniques or controlled self-assembly [34,99,116]. The use of LSPR for refractive index sensing offers promising opportunities in terms of limit of detection and sensitivities, which can be further enhanced by exploiting the large electromagnetic field enhancement in the surroundings of the NPs to amplify external signals, such as Raman scattering and fluorescence, by serving as nanoantennas. Several SERS- and MEF-based biosensors have been recently proposed in the form of both periodic and non-periodic nanoarrays, achieving very promising results in the biosensing field [26,30]. Although plasmonic nanoarrays for SERS-based biosensors have been extensively reviewed in recent years [117,118], it is worth mentioning some

of the most recent SERS-based nanostructured surfaces for cancer biomarker detection. In this frame, Muhammad et al. [119] reported on a gold NP array functionalized with a DNA aptamer for SERS detection of interleukin-6 (IL-6), an important inflammatory and cancer progression cytokine. The recognition of the target IL-6 in serum is achieved by the conformational change of the aptamer, resulting in the corresponding change of the output Raman intensity ratio (I_{660}/I_{736}). The proposed nanoarray is reported to work in the IL-6 dynamic range of 10^{-12} – 10^{-7} M (Figure 4a). This example further elucidates the applicability of SERS substrates for real samples (blood, serum, urine) with no nonspecific signal detection. Most of the published top-down fabrication strategies allow regular, densely packed, and periodic geometries with strong electromagnetic field confinement, which represent the ideal candidates for plasmonic sensing. Despite this, large efforts have been the method to obtain similar performance starting from the self-assembly of monolayers of bottom-up synthesized plasmonic NPs. For example, Kang et al. [120] developed a closely-packed and ordered Au octahedra array as a highly active and reliable SERS substrate for miRNA detection, which is another hot topic in the biosensing community. The synthesis of Au octahedra was performed via bottom-up chemical synthesis, and the monolayer was achieved by exploiting interfaces between two immiscible liquids. The proposed sensor achieved an miRNA concentration down to 5.3 aM (LOD), a broad dynamic range (from 10 aM to 10 nM) without any signal amplification strategies, and discriminated targets differing from one another by only a single nucleotide. Among the many available SERS nanoarrays, more exotic nanostructures for the amplification of the Raman signals are not missing. For example, Chen et al. proposed a 3D nanopopcorn plasmonic substrate fabricated by a thermal evaporation method. After functionalization with a specific aptamer DNA, it was exploited for the highly sensitive and reproducible detection of the influenza A/H1N1 virus. They exploit the surface energy difference between the perfluorodecanethiol (PFDT) spacer and Au layer to self-assemble gold NPs in a highly uniform way.

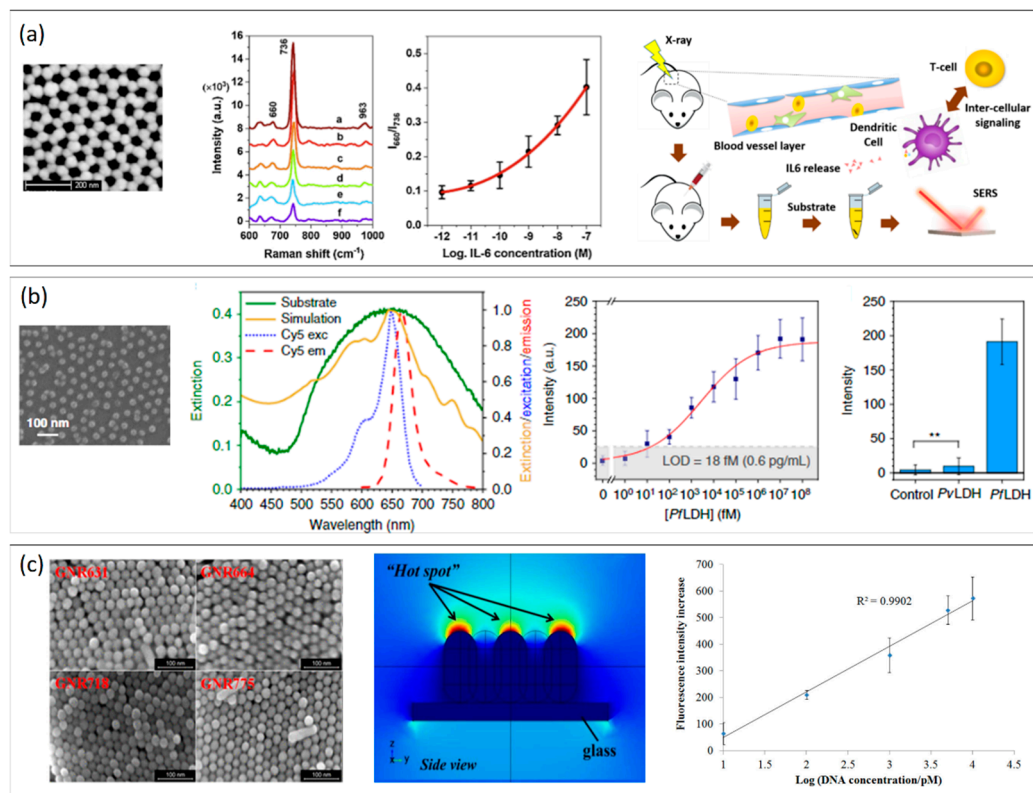


Figure 4. (a) From left to right: SEM image of a gold NP nanoarray for SERS detection of IL. The SERS signals prove the recognition of the target IL-6 in serum via corresponding changes of the output Raman intensity ratio (I_{660}/I_{736}) in the concentration range 10^{-12} – 10^{-7} M. The proposed nanoarray

is reported to give results comparable to ELISA tests in serum. Adapted with permission from Ref. [119]. Copyright (2021), Elsevier. (b) From left to right: SEM image of the AuNP hexagonal array self-assembled on the top of a glass coverslip; experimental extinction spectrum of the substrate (green continuous line) and theoretical simulation of the optical response provided by the substrate morphology as measured by SEM (gold continuous line); on the same graph, the excitation and emission peaks of Cy5 (blue and red dashed lines) are reported; calibration curve (fluorescence intensity vs. PflDH concentration in spiked human blood) of the immunoassay for PflDH concentration in the dynamic range from 35 fg/mL to 3.5 µg/mL. The MEF substrate is reported to be highly specific, as confirmed by specificity tests (** p -value < 0.001). Adapted with permission from Ref. [35], Copyright (2020), Springer Nature. (c) From left to right: SEM image of gold nanorods (GNRs) of different sizes; simulation of the electromagnetic field distribution of the gold nanorods array (side view). Calibration curve of GNR nanoarray-based DNA chip as a function of the increasing target ssDNA concentration. Adapted with permission from Ref. [121]. Copyright (2017), American Chemical Society.

The neighboring nanoparticles created a high density of plasmonic hotspots on the substrate, enabling reproducible target molecule analysis. When the target A/H1N1 virus was added onto the substrate, the coupling between aptamer DNA and the virus decreased the Raman signal intensities. Such variation was used for the highly accurate quantitative evaluation of the A/H1N1 virus. The LOD and assay time were estimated to be 97 PFU/mL and 20 min, respectively [122]. These are just some examples of the powerful applications of SERS nanoarrays in biosensing, which can be performed with very promising results, both in label-free mode and by using Raman reporters to reduce signal-to-noise ratios and LODs. Another signal that has been proved to be largely amplified by interaction with plasmonic nanoarrays is doubtless fluorescence. Metal-enhanced fluorescence or plasmon-enhanced fluorescence has been widely investigated to boost biomolecular fluorescence-based detection down to the single-molecule resolution, solving the very general issues of sample-autofluorescence, signal-to-noise ratio, and interfering signals [123]. MEF for biochemical sensing has paved the way to more irregular plasmonic nanoarrays, since the broader the plasmon peaks, the more probable the spectra overlap with a selected fluorescent dye. Therefore, the quest for MEF-based biosensors is to achieve a sufficiently large plasmon that could overlap with both excitation and emission spectra of a fluorescent dye in a dual-mechanism amplification scheme [35]. What instead must be carefully tuned is the distance between the plasmonic nanostructures and the fluorescent dyes by using spacers to functionalize the nanoarrays and achieve the desired distance. In this regard, a biosensor capable of detecting IgG concentration has been obtained by a mixed top-down/bottom-up fabrication strategy to produce gold nanoislands on an etched substrate (AuNIs) [34]. The proposed nanoarray was functionalized by a self-assembled monolayer of alkanethiol and used for IgG detection, followed by covalent immobilization of the antibodies. The sandwich structure was completed by incubating the sensor surface with fluorescently labeled antibodies, and thus detection of the analyte of interest is achieved. Different fabrication thicknesses for the AuNIs were analyzed, but finally, the choice fell on those that allowed the peak LSPR to be observed at the excitation/emission maximum of the fluorophores chosen for analysis. The LOD of the biosensor based on metal nanostructures is 4.3 ng/mL, which is a very good result for biomedical analysis, showing the potential application of a large-scale, low-cost fabrication strategy to significantly reduce the LODs of a target analyte. Another very interesting application of MEF-based nanoarrays concerns the diagnosis of sepsis. Sepsis is a complication of an infection, and its evolution can be very serious. Without immediate treatment and diagnosis, it can lead to death. In the United States, its mortality rate exceeds that of prostate and breast cancer [124]. All this can be combated by early diagnosis, for example with biomarkers that are closely related to sepsis, namely procalcitonin (PTC), interleukin, and lactate, with their respective sensitivity/specificity values [125,126]. In this context, a rapid, point-of-care (POC) testing device has been developed that allows the quantifi-

cation of PCT, aiding in the diagnosis of sepsis. Again, this takes advantage of the LSPR superposition of a nanoarray, and the excitation spectrum of fluorescent dyes. For this application, periodically ordered gold nano-pillars of 140 nm square and 320 nm pitch are fabricated on glass substrates. QDs are used as fluorescent dyes. The gold nanochip was fabricated by e-beam lithography or nanoimprinting [127]. The gold nanochip was integrated into a low-cost microfluidic chip sandwiched with PMMA polymer, where the analyte sampling and bioassay flow, are controlled by a peristaltic pump. For PCT detection, an anti-PCT monoclonal antibody was immobilized on the surface of the gold nanopillars, following which a PCT solution was injected into the gold chip fixed in the microfluidic support. At this point, a solution of biotin-conjugated PCT detection antibody was injected, followed by the application of QD-655-conjugated streptavidin. A laser and CCD camera controlled via LabVIEW was used for fluorescent signal detection of QDs. This POC device showed very high performance as it entered 30 min to perform the assay and the data analysis. The LOD calculated was 0.5 ng/mL, which is within clinical limits for sepsis diagnosis. A large-scale nanofabrication approach for MEF-based plasmonic nanoarrays was also proposed by Minopoli et al. [35]. In this work, a gold NP array was made by block copolymer micelle nanolithography (BCMNL) for the specific and ultrasensitive detection of *Plasmodium falciparum* lactate dehydrogenase (PfLDH)—a malaria marker—in whole blood. The device achieved a limit of detection smaller than 1 pg/mL with very high specificity without any sample pretreatment (Figure 4b). The nanoarray optical response was tuned to achieve the highest Cy5 fluorescence enhancement by exploiting a dual enhancement mechanism in which both dye excitation and emission fall in the extinction of the NP array, offering a versatile tool for biochemical sensing and diagnosis of diseases. Tang et al. [121] proposed, instead, an innovative gold nanorod array biochip to systematically investigate the localized surface plasmon resonance (LSPR)-coupled fluorescence enhancement for signal amplification in molecular beacon detection. Their nanorods were assembled in an ordered vertical standing array on a glass substrate, resulting in dramatically intensified LSPR between adjacent nanoparticles as compared to that from an ensemble of random nanorods. They experimentally proved the dependency of the metal-enhanced fluorescence on the distance between metal nanostructures and fluorescent dye (Figure 4c). The applicability of their nanoarray was extended to molecular fluorescence enhancement as a highly functional and ultrasensitive plasmonic DNA biochip as a molecular beacon. A summary of Plasmonic Nanoarrays for MEF- and SERS-based biosensors is provided in Table 3.

Table 3. Plasmonic nanoarrays for MEF- and SERS-based biosensors.

Material	Array Structure	Detection Method	Analyte	Linear Range	LOD	Ref.
Gold	Nanoparticles	SERS	Interleukin-6	10^{-12} – 10^{-7} M	0.8×10^{-12} M	[119]
Gold	Closely-packed octahedra array	SERS	let-7a miRNA	10 aM to 10nM	5.3 aM	[120]
Gold	3D nanopopcorn	SERS	influenza A/H1N1 virus	0–75,000 PFU/mL	97 PFU/mL	[122]
Gold	Nanoislands	MEF	Alexa Fluor [®] 546-IgG	4.3–1000 ng/mL	4.3 ng/mL	[34]
Gold	Nanoislands	MEF	PE-Cy7-IgG	30.4–1500 ng/mL	30.4 ng/mL	[34]
Gold	Nanopillars	MEF	procalcitonin	0.1–10 ng/mL	0.5 ng/mL	[127]
Gold	Nanoparticles	MEF	<i>Plasmodium falciparum</i> lactate dehydrogenase	35 fg/mL to 3.5 µg/mL	1 pg/mL	[35]

4. Plasmonic Polymer Nanocomposites for Biomedicine

Usually, polymer nanocomposites are realized to reinforce the mechanical or structural properties of the polymer basic material [128]. Conversely, the polymer matrices can embed plasmonic NPs to gain new optical properties without considerably modifying their mechanical properties. Plasmonic nanocomposites are emerging as novel platforms for biomedical applications due to their potentiality in the fabrication of large-scale plasmonic nanocomposites. Since the environment deeply affects the optical properties of NPs, the dispersion and aggregation of the NPs in the polymer matrix are the key challenges for the fabrication of plasmonic nanocomposites. Generally, three main fabrication techniques are involved in the fabrication of polymeric plasmonic nanocomposites: (i) deposition or self-assembling of plasmonic NPs on the surface of transparent polymers, such as polydimethylsiloxane (PDMS) [129,130], poly (methyl methacrylate) (PMMA) [131], and poly (ethylene terephthalate) (PET) [132]; (ii) preparation of a pre-polymer solution containing plasmonic NPs, which can be processed by thermal curing [133,134], photopolymerization [135], or collected in the form of nanofibers using electrospinning [133,136]; and (iii) in situ reduction of metal salts on or within polymeric matrices [136,137]. Among the many available polymers, hydrogels have recently played an important role in the field of biomedicine [138]. The 3D network of hydrogels and the large content of water they can potentially accommodate make them the ideal candidates for the formation of scaffolds to be used for in vitro cell culturing and for in vivo wound healing patches [139,140]. Moreover, they are generally considered as biocompatible and biodegradable, while offering a large variety of physicochemical and mechanical properties [141]. Hydrogels present good anti-fouling properties and tend to preserve the activity and functionality of biomolecules within their network, offering great potential also in biosensing applications [142,143]. Their 3D networks can be made *stimuli*-responsive inducing a controlled swelling or shrinkage as a function of external parameters (e.g., pH, temperature, ionic strength, etc.) [144,145]. In this context, the combination of plasmonic NPs with hydrogels offers new insights in biomedical applications due to their optomechanical properties.

Plasmonic Hydrogel Nanocomposites for Biomedicine

While Heilmann has largely discussed NP dispersion in rigid polymers in [146], the use of hydrogels as containing material is currently the object of several studies for their capability to respond to chemical and physical *stimuli*, such as hydration, pH, ionic strength, specific chemical interactions, temperature, light, magnetic fields, and so on. Indeed, the application of this group of polymeric material widely ranges from optical data recording and storage to soft actuators, from therapeutic platforms to biosensing [147–149]. In particular, in the field of biomedicine, thermal care, tissue engineering, and drug delivery, sensing and imaging for diagnostics and biology commonly use polymeric nanocomposites based on hydrogels and NPs. Therefore, the combination of these smart hydrogels with functional plasmonic NPs adds synergistic benefits to the composite system [41]. Embedding plasmonic NPs in thermally responsive hydrogels opens to a wide range of applications in theranostics. The combination of NPs that can efficiently convert light absorption in temperature increase, with thermally responsive hydrogels has been employed as actuator/sensing systems, in thermal therapy, and as light-triggered materials [150–153]. As an example of photothermal actuator/sensing systems, in [150], Au nanorods have been embedded in gelatin hydrogel functionalized with anti-epithelial cell adhesion molecule (anti-EpCAM) to capture and release on demand circulating tumor cells. In this system, light absorption was converted into temperature energy by Au nanorods that melted the gelatin and decreased the adhesion of cells to the hydrogel. Several works have been presented in the field of photothermal and photodynamic therapy using PNP, but the combination with a hydrogel as the collagen presents the advantage of combining the thermal therapy triggered using plasmonic NPs and the localized delivery by collagen injection. Collagen is a perfect biocompatible and thermomechanical responsive material widely used in cancer therapy [151]. Among the thermoresponsive hydrogels that exhibit

shape memory effect, i.e., polymers that temporarily and elastically change their shapes with heating, poly(N-isopropyl acrylamide) (pNIPAM) has been widely studied because of its large swelling ratio in a sharp phase transition [133,152–155]. In pNIPAM, dimensions significantly change with temperature, and then the inclusion of Au NPs in them produces a hybrid nanocomposite with on-demand shape-morphing properties. In [154], authors fabricate valves using two kinds of plasmonic NPs embedded in poly(NIPAM-co-acrylamide), namely Au nanospheres and nanoshells, absorbing at 532 and 832 nm, respectively. In this way, the microfluidic device has two independent controlled valves. Furthermore, microactuators can be fabricated by exploiting the pNIPAM and NPs, when the system is illuminated with a patterned light by an optical fiber [153] or an optical mask [133,154]. In this way, it was possible to move the actuator by locally illuminating and then remotely controlling the swelling/deswelling of the hydrogel. Moreover, a 3D structure could be generated by the photothermal fabrication of a thermo-crosslinking material as the poly(NIPAM-co-acrylic acid derivative) hydrogels [156]. Sensing with plasmonic hydrogel nanocomposites can be achieved by exploiting all the sensing mechanisms highlighted in the previous sections: the sensitivity to RI in the immediate NPs surroundings [157,158], the NPs aggregation in LSPR-based sensing [25,159], the SERS effect for a label-free detection [160], or the MEF mechanism for labeled biomolecules [36]. As stated in the previous sections, in LSPR sensing, gold NPs are usually preferred to silver NPs because they generally show a lower oxidative susceptibility than Ag NPs, which occur when they come in contact with solvents and biomolecules [21,161]. Moreover, the functionalization and the biocompatibility of Au NPs have been widely documented [104,162]. Unfortunately, the colloidal NP aggregation requires several stabilization steps to avoid non-specific aggregation. For example, degradation and/or spontaneous aggregation of citrate AuNPs occurs in the presence of salts (i.e., NaCl solutions, phosphate-buffered saline (PBS) or K buffer), of organic solvents, and strongly acidic or basic pH [94,95,163]. Moreover, NP aggregation sensing is generally developed in colloidal solutions, which severely limits its practical application. To overcome chemical stability problems and oxidative susceptibility of silver nanoparticles, a promising strategy has been the inclusion of plasmonic NPs within hydrogels [158,164,165]. These platforms have been proven to preserve NP stability and maintain their optical functionality as plasmonic sensors. Moreover, plasmonic NPs embedded in polymeric materials do offer a promising strategy to overcome the expensive, complex, and time-consuming fabrication techniques generally required to produce sensitive plasmonic nanoarrays. Furthermore, 3D nanocomposites give rise to nanoplatforms with enhanced surface-area-to-volume *ratio*, analytical performance, and physicochemical stability of functionalization NPs [166–168]. In [158], a 3D nanocomposite hybrid platform based on the combination of citrate gold NPs and poly-(ethylene glycol) diacrylate (PEGDA) hydrogel was proposed for LSPR biosensing. By exposing the proposed flexible nanocomposite to buffers and organic solvents, the authors showed that the stability of gold NPs increased when embedded in the hydrogel network compared to the corresponding colloidal aqueous solutions. Moreover, the optical detection of biotin was proved by modifying with a cysteamine the Au NPs embedded into the nanocomposite. Recently, Miranda et al. [36] presented another PEGDA-based biosensor containing spherical citrate-gold NPs able to detect the biotin–streptavidin (SA) interaction down to 10^{-12} M concentrations. The originality of the sensor pointed to the fabrication strategy that provided a large-scale, versatile, easy, and low-cost biosensing flexible platform with applications in biomedical or environmental diagnostics. The innovative hydrogel-based sensor was optically stable due to the enhancement of stability of the embedded citrate-gold NPs. In this case, the changes in the absorption spectrum result from the large swelling of the high molecular weight PEGDA interacting with solutions containing molecules with high molecular weight. Moreover, it provides dual-optical sensing; the quantitative determination of the analyte exploits both LSPR and metal-enhanced fluorescence of Cy3-labeled SA using biotin functionalized NPs for MEF-based sensing (Figure 5a). Similarly, a biosensor with a quantitative LSPR response based on polyvinyl pyrrolidone (PVP) hydrogel and silver NPs functionalized

with glucose oxidase (GOx) was presented in [165]. A decrease in NP absorption spectrum proportional to the concentration of glucose was reported and explained by the increase in the distance between the NPs. In fact, due to the high affinity of glucose and GOx and the presence of the anionic reduced FAD species, an enhancement in the swelling ratio of the hydrogel was observed, and the NPs' average distance increased proportionally with the concentration of glucose, thus affecting the optical spectrum. The high sensitivity of the sensor led to an LOD of 10 pM. Among the hybrid colorimetric sensors, the one proposed in [169] showed a strong shrinkage and color variation in the presence of the influenza A virus. The proof of concept was fabricated from a prepolymer solution with diazide-poly(ethylene) glycol (PEG) with 6 kDa molecular weight and polyol-based hydrogel of dendritic polyglycerol cyclooctyne (dPG) with 10 kDa molecular weight. Finally, sialic acid stabilized Au NPs were incorporated into the hydrogel during polymerization. The resulting sensor exhibited high specificity and affinity for the hemagglutinin protein present in the influenza A virus. The combination of NPs with hydrogels has been adapted also for SERS sensing. Hydrogels allow the trapping of NPs, forming many hotspots, and the analyte is free to access the NPs through diffusion while using 3D physical supports. One hydrogel–NP combination used for SERS-based sensing is that which exploits the reversibility properties in drying and rehydration of agarose together with the sensing properties of silver NPs [170,171]. In particular, the reversibility of agarose is exploited to promote the mobility of the NPs to use them as dynamic hotspots. At the same time, the porosity of the agarose acts as a physical trap for the analyte molecules, which can be also released with rehydration. Furthermore, SERS-based hydrogel–NP nanocomposite systems can be used for sensing and imaging. In this case, the three-dimensional data were added to the quantitative relationship, since the hydrogel blocked the sensitive plasmonic NPs and detected the position data together with the quantity of analyte. Furthermore, systems consisting of pNIPAM and Au nanorods have been studied in [172] and [137]. In particular, in [172], a bacterial culture of *Pseudomonas aeruginosa* was incorporated in pNIPAM, containing in turn Au NPs functionalized for the detection of pyocyanin, closely related to the quantity of biofilm.

In this case, pNIPAM was shown to be compatible with the biofilm culture and allowed the diffusion of nutrients. However, the 3D data resolution was affected by the biofilm growth and the high diffusion properties of pNIPAM involving the pyocyanin position. A similar system was used in [137] for the detection of two different and coexisting bacterial colonies trapped in an agar multilayered system in which thin agar layers were alternated with layers decorated with Au NPs. In particular, the decorated agar layers were used for the quantitative and positional detection of pyocyanin and violacein, produced by *P. aeruginosa* and *Chromobacterium violaceum*, respectively. In this case, the diffusivity of the agar, which was lower than that of the pNIPAM, allowed a better spatial resolution proven by the correct identification of the specific biofilm, while still allowing the right supply of nutrients. Finally, in [173] a similar successful multiplexing sensing platform was designed by using Ag NPs embedded in circular and square PEGDA microparticles coated or functionalized to detect human serum albumin (HSA) and glucose, respectively. Shaped PEGDA microparticles were realized by photolithography and then decorated with Ag NPs, and finally appropriately coated/functionalized. The selectivity was confirmed by Raman mapping, where different shape microparticles reveal different spectral patterns. The proof of concept was performed in assay with concentrations ranging in the dynamic range from 1 pg/mL to 1 µg/mL for both glucose and HSA. No crosstalk was detected (Figure 5b). Therefore, the field of plasmonic polymer nanocomposites is offering several strategies for the detection of different biomarkers with features combining both plasmonic colloids and nanoarrays, and with LODs and sensitivities comparable to them.

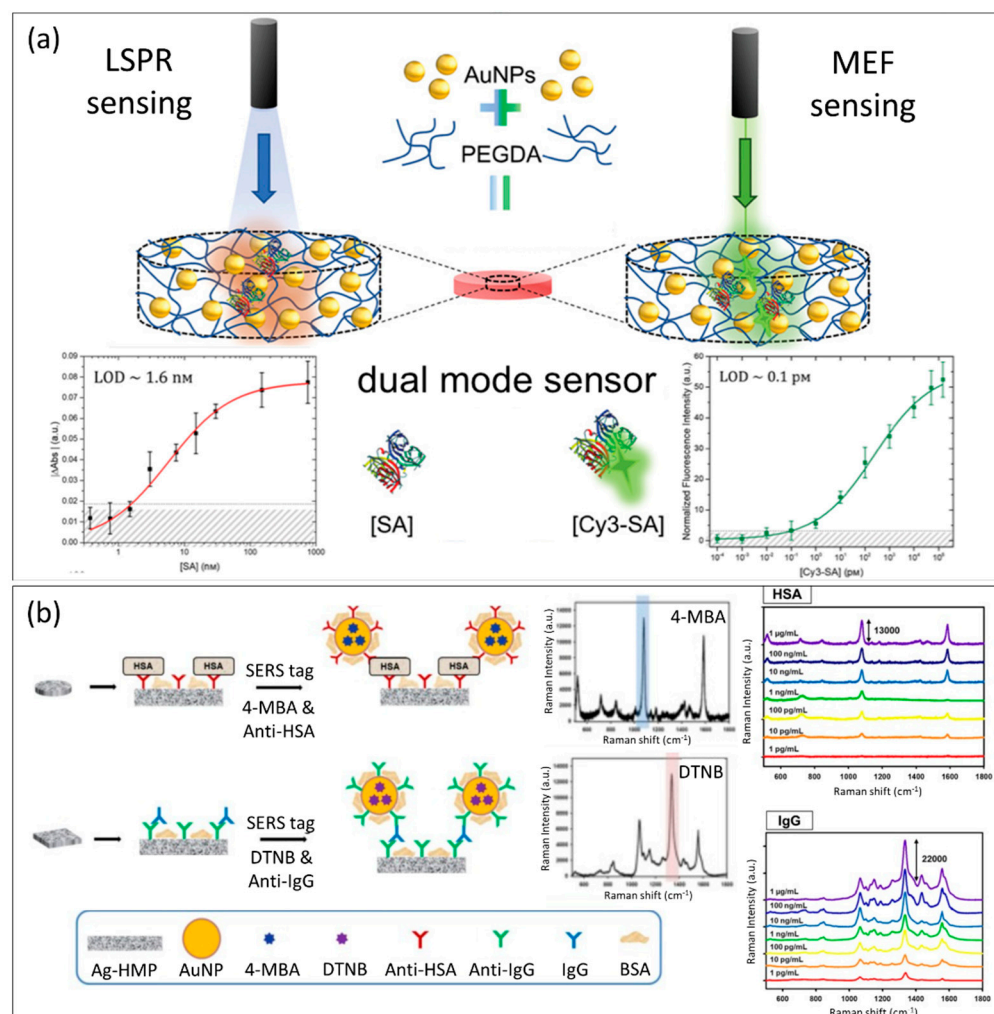


Figure 5. (a) Schematic representation of the dual mode plasmonic hydrogel transducer based on PEGDA and spherical gold NPs. On the left, the label-free sensing of streptavidin concentration [SA] is realized by absorption spectroscopy of the gold NPs functionalized with biotin. The absorbance variations as a function of the streptavidin concentration are due to the swelling of a high molecular weight hydrogel. On the right, the sensing of the Cy3-labeled streptavidin concentration [Cy3-SA] is realized by metal-enhanced fluorescence sensing mode. Adapted from Ref. [36]. Copyright (2022) The Authors. *Advanced Materials Technologies* published by Wiley-VCH GmbH. This article is distributed under a Creative Commons Attribution (CC-BY) license. (b) Immunoassay using Ag nanoparticles/hydrogel microparticles and SERS nanotag. On the left, a schematic illustration of the immunoassay process for the detection of target proteins is reported. On the right, SERS spectra acquired from a sandwich immunoassay using different concentrations of HSA and IgG are illustrated. Adapted with permission from Ref. [173], Copyright (2021), Elsevier.

5. The Evolution of Plasmonic Nanosensors: The Role of Microfluidics and Microelectronics for Point-of-Care Testing Devices

In recent years, an increasing demand for portable biosensors has been observed. Among optical biosensors, plasmonic biosensors represent the most developed biosensing technology [174–176]. However, in order to produce point-of-care (POC) devices that exhibit easy modes of use, compact size, and limited cost, it is important to combine the LSPR biosensor with microfluidics and microelectronics [177,178]. The coupling of optics and microfluidics offers several advantages. Microfluidic chips are used to consume small volumes of reagents and samples and show a higher efficiency due to short mixing times and fast system responses (Figure 6a). The advantages of integrating LSPR chips with

microfluidic systems also include miniaturization, low cost, and high throughput [179–182]. Finally, this combination can enable simultaneous analysis and processing of multiple analytes [183]. One must, furthermore, add data processing technologies and visualization of the analysis results. CMOS electronics and smartphones are the possibly exploitable technologies to succeed for this purpose (Figure 6b). In particular, smartphone-based optical biosensors perform the high quality of the integrated camera as a detector, replacing expensive spectrophotometers and laboratory microscopes [184]. However, to commercialize these devices, many aspects have to be optimized. First, optical biosensors are sensitive to changes in environmental conditions that affect signal stability. The reproducibility of the signal must be guaranteed by the optical connections, and the reproducibility of the transduced signal must be guaranteed by the smartphone. A crucial point is to create a reliable and stable connection to work with common smartphones. The smartphone, not being managed by professionals, should be easy-to-use, providing readable results. In addition, smartphones from different manufacturers can often have diverse characteristics, which lead to statistically different results. Therefore, more tests to validate the goodness of the optical device on various smartphones are needed. Secondly, the application installed on the smartphone should be user-friendly and return univocal results. The first example of these systems for the real-time detection of proteins, such as transferrin and immunoglobulin (IgG), is presented in [185]. In detail, a plasmon resonance sensor was fabricated using 1.5 cm long capillaries and AuNPs. The capillaries were treated with a Piranha solution, and then their surface was treated with different chemicals by capillarity, first with PDDA (diallyl dimethylammonium chloride), and then with sodium-p-styrenesulfonate (PSS), allylamine hydrochloride (IPA), and PAH. The positively-charged capillaries easily accommodate AuNPs. Next, the LSPR capillary platform was functionalized via MUA and immersed in an aqueous solution of EDC/NHS for 30 min. Finally, the sensor was immersed in an aqueous anti-transferrin/protein A solution of 0.1 mg/mL, rinsed with phosphate-buffered saline (PBS, pH 7.4), and blocked using bovine serum albumin (BSA, 0.1 mg/mL). The structure of the plasmonic detection device included two connectors, which linked two optical fibers to the capillary LSPR sensor, which were then together connected to a LED, whose selected emission wavelength was 595 nm. Two complementary metal-oxide semiconductor (CMOS) image sensors connected to a laptop were used to monitor the light scattered through the capillary walls, the transmitted light, and the light exiting the optical fibers. The sidewalls of the capillaries and the ends of the fibers were selected as regions of interest (ROIs). Labview software was used for data acquisition, processing, and ROI selection. The intensity of the ROI was exploited to calculate the LSPR response of the sensor. With the system on, all the images were captured and processed. To detect the interaction between antibody and antigen, transferrin and IgG were diluted in PBS and injected into the reference channels. When the antibody binds to the antigen on the surfaces of the AuNPs, an increase in the refractive index around the particles' surfaces occurs. The intensity of the optical response in the ROI of the capillaries' sidewalls increases only if the antibody is present. The combination of the LSPR sensor and CMOS technology is well suited for the detection of multiple analytes. Another example of an integrated optics and microfluidics sensor was developed for real-time cytokine biomarker detection [186]. In this case, the sensor was developed with eight parallel microfluidic channels, orthogonal to six meandering strips of antibody-functionalized ensemble AuNRs. Six functionalized AuNR strips were conjugated with six different cytokines: interleukin-2 (IL-2), interleukin-4 (IL-4), interleukin-6 (IL-6), interleukin-10 (IL-10), interferon-gamma (IFN- γ), and tumor necrosis factor-alpha (TNF-R). By using dark-field imaging scanning optics, it is possible to visualize scatter light intensity next to the AuNRs array. This sensor can monitor the inflammatory response of newborns after cardiopulmonary bypass surgery (CPB) by monitoring changes in their serum cytokines over time. This device overcomes the recurring technical limitations and shows a high sensitivity of cytokines up to 520 pg/mL concentrations. Another important application of these point-of-care devices concerns drug dosing. A handheld and portable setup that exploits the phenomenon of transmission-

localized surface plasmon resonance (T-LSPR) is presented [187]. This novel device is composed of off-the-shelf components. The T-LSPR setup consists of gold nanoislands (AuNIs) functionalized with specific aptamers to recognize the antibiotic tobramycin. The microfluidic structure consists of a slide with the AuNIs and two independent channels. AuNIs were realized on a pre-coated slide with FTO (fluorine-doped tin oxide) to ensure stability (Figure 6c). An in-depth description of the realization of this technology can be found in Refs. [188,189]. To subsequently functionalize the surface of the AuNIs, the covalent sulfur–gold interaction is exploited. After this process, the slides are incubated for sixteen hours with tobramycin-specific DNA aptamer solutions in PBS. The measurement set-up consists of white light LED and a CMOS image sensor. The measurement process is straightforward, as the transmitted light through the spindles, which contains information about the plasmonic phenomenon, arrives at the CMOS detector through a lens. For this reason, the CMOS sensor plays a fundamental role. Thanks to that, it is possible to photograph a large area and distinguish the different regions; this will be useful for the last analysis. This device, contained in a small 3D printed case, can detect, in real-time, up to $0.5 \mu\text{M}$ tobramycin and represents an evolution in the field of biosensing and real-time monitoring of drug dosages. Another device, able to overcome the limitations of the developing point-of-care devices based on the LSPR phenomenon, is presented in [190]. Integrating the microfluidic chips with the POC systems and the LSPR chips is one of the biggest problems, along with increasing the sensing sensitivity and the mass fabrication of metal nanostructures on the substrate.

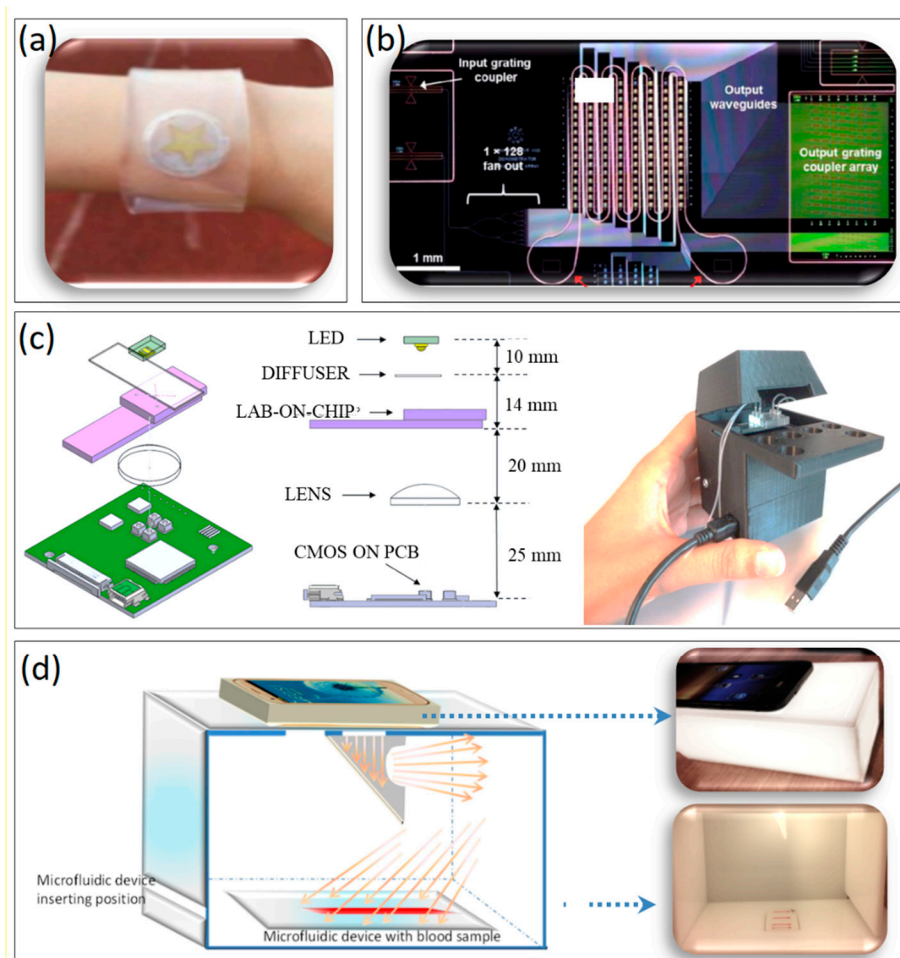


Figure 6. (a) LSPR wearable colorimetric sensor to detect humidity. Adapted with the permission from Ref. [177], Copyright (2017), John Wiley and Sons. (b) Microscope image of a sensor made to acquire

128 real-time optical sensor outputs simultaneously. Adapted with the permission from Ref. [183]. Copyright (2019), Elsevier. (c) From left to right: schematic representation of the T-LSPR set-up, side view with relative distances between components, and final complete device. Adapted with the permission from Ref. [187]. Copyright (2015), American Chemical Society. (d) Schematic representation of the microfluidic device and its realization for colorimetric analysis of blood hematocrit. Adapted with the permission from Ref. [191]. Copyright (2017), Elsevier.

The presented device overcomes some of these limitations and problems. In fact, for one thing, the plasmon shift is not monitored, but the plasmon field excites a fluorescence signal of the dyes bound to the analyte, improving the detection sensitivity up to 10 times. To maximize the fabrication of metal nanostructures, a printed 4" nickel wafer was fabricated by electroplating. The process is well described in [192]. The metal structures that allow for the exploiting of the LSPR phenomenon are gold nanopores, and the fluorophore Alexa-Fluor 647 was used. In this particular case, immobilization of the anti-PSA antibody led to revealing the presence of PSA. The technique used for immobilization is dual polarization interferometry. To realize the POC system, a microfluidic chip was inserted into a system of micro-pumps controlling the flow. This POC system, unlike others, is very compact, so much so that a smartphone camera can be used as a CMOS imaging IC. Kim et al. presented a smartphone-based sensor for colorimetric analysis of hematocrit with an LOD of 0.1% [191]. In this case, the smartphone camera catches images of the blood present in the microchannel, and the resulting data are analyzed using a dedicated app. Specifically, the blood was diluted with plasma to have different hematocrit concentrations and then loaded into the microchannel with a PDMS micropump. Blood images were processed by the grey-scale-valuation relative to each pixel, which increases as the hematocrit levels increase (Figure 6d). The presented work is an example of how, once again, the optical platform, microfluidics, and smartphone can work together to make POC devices. Considering those just listed, it is clear how the use of those technologies can benefit the process of diagnosis and drug-dosing by making the process faster, more reliable, and easier to access for everybody.

6. Conclusions and Future Perspectives

In this review, we reported on the fabrication, characterization, and application of plasmonic nanomaterials in biomedicine, mainly focusing on biosensing, bioimaging, and drug delivery monitoring. We summarized colloid, nanoarray, and hydrogel nanocomposites design and engineering to produce diagnostic platforms to be operated in vitro as well as in vivo, which are easy-to-use, highly specific, and sensitive. We highlighted the tendency of researchers to push down the LOD and accuracy of the proposed platforms and to still keep low costs. It was demonstrated that the intrinsic optical features of plasmonic nanoparticles are strongly dependent on the size, shape, and composition of the NPs themselves, which can be tuned according to the desired applications. For instance, NPs exhibiting sharp plasmonic resonances are the ideal candidates to design LSPR-based sensors; the figure of merit (*FOM*) clearly describes the capability of an optical transducer to undergo a measurable peak shift even for very small changes of the refractive index. Vice versa, plasmonic NPs with broad resonances (with large FWHM) represent the ideal plasmonic nanoantennas for external signal amplification (SERS and MEF-based sensing mechanisms). Despite all the reported fabrication strategies and ultra-high performances achieved by the proposed devices, it seems that the technology transfer remains the main bottleneck of the establishment of plasmonics as a gold standard in the biosensing community [193]. Therefore, the real application of the described devices will be possible only when the proposed technologies will be made intuitive, largely understandable, and reliable, also by non-specialized personnel. Moreover, the integration of these devices within microelectronics and microfluidics components could represent the best strategy to evolve from a simple transducer to a smart point-of-care testing device encompassing rapid, easy-to-handle, and portable devices, which could give affordable results by using tiny volume samples, thus reducing the invasiveness of the gold standard biochemical assays. We expect that

plasmonic transducers based on colloids, nanoarrays, and nanocomposites will become a leading technology in biomedical applications in the next years.

Author Contributions: Conceptualization: L.D.S., and I.R.; writing and original draft preparation of Section 1: V.N., C.T., and B.M.; writing and original draft preparation of Section 2: V.N., G.C., and C.T.; writing and original draft preparation of Section 3: V.N., and B.M.; writing and original draft preparation of Section 4: B.M., and P.D.; writing and original draft preparation of Section 5 and 6: V.N., B.M., and G.C.; review and editing: B.M., I.R., C.T., G.C., P.D., and L.D.S.; supervision: I.R., and L.D.S. All authors have read and agreed to the published version of the manuscript.

Funding: Luca De Stefano and Ilaria Rea acknowledge the partial financial support from the National Research Council (CNR) with Projects@CNR: SAC.AD002.173.026 TIPPS (tracking and identification of asymptomatic Patients through engineered antibodies bioconjugated plasmonics in a Pandemic Scenario) and SAC.AD002.173.025 Seeinvis (SERS-based biosensor for virus recognition).

Data Availability Statement: Not applicable.

Conflicts of Interest: The authors declare no conflict of interest.

References

1. Gormley, A.J.; Larson, N.; Sadekar, S.; Robinson, R.; Ray, A.; Ghandehari, H. Guided delivery of polymer therapeutics using plasmonic photothermal therapy. *Nano Today* **2012**, *7*, 158–167. [[CrossRef](#)] [[PubMed](#)]
2. De Tommasi, E.; Esposito, E.; Romano, S.; Crescitelli, A.; Di Meo, V.; Mocella, V.; Zito, G.; Rendina, I. Frontiers of light manipulation in natural, metallic, and dielectric nanostructures. *Riv. Nuovo Cim.* **2021**, *44*, 1–68. [[CrossRef](#)]
3. Miranda, B.; Rea, I.; Dardano, P.; De Stefano, L.; Forestiere, C. Recent Advances in the Fabrication and Functionalization of Flexible Optical Biosensors: Toward Smart Life-Sciences Applications. *Biosensors* **2021**, *11*, 107. [[CrossRef](#)]
4. Jayanthi, V.S.P.K.S.A.; Das, A.B.; Saxena, U. Recent advances in biosensor development for the detection of cancer biomarkers. *Biosens. Bioelectron.* **2017**, *91*, 15–23. [[CrossRef](#)]
5. Fontana, F.; Liu, D.; Hirvonen, J.; Santos, H.A. Delivery of therapeutics with nanoparticles: What's new in cancer immunotherapy? *Wiley Interdiscip. Rev. Nanomed. Nanobiotechnol.* **2017**, *9*, e1421. [[CrossRef](#)]
6. Yougbaré, S.; Chou, H.L.; Yang, C.H.; Krisnawati, D.I.; Jazidie, A.; Nuh, M.; Kuo, T.R. Facet-dependent gold nanocrystals for effective photothermal killing of bacteria. *J. Hazard. Mater.* **2021**, *407*, 124617. [[CrossRef](#)]
7. Chen, Y.-T.; Lee, Y.-C.; Lai, Y.-H.; Lim, J.-C.; Huang, N.-T.; Lin, C.-T.; Huang, J.-J. Review of Integrated Optical Biosensors for Point-of-Care Applications. *Biosensors* **2020**, *10*, 209. [[CrossRef](#)]
8. Sin, M.L.; Mach, K.E.; Wong, P.K.; Liao, J.C. Advances and challenges in biosensor-based diagnosis of infectious diseases. *Expert Rev. Mol. Diagn.* **2014**, *14*, 225–244. [[CrossRef](#)]
9. Crisci, T.; Falanga, A.P.; Casalino, M.; Borbone, N.; Terracciano, M.; Chianese, G.; Gioffrè, M.; D'Errico, S.; Marzano, M.; Rea, I.; et al. Bioconjugation of a PNA Probe to Zinc Oxide Nanowires for Label-Free Sensing. *Nanomaterials* **2021**, *11*, 523. [[CrossRef](#)]
10. Chianese, G.; Terracciano, M.; Moretta, R.; Cappiello, P.; Vitiello, G.; Aronne, A.; Schiattarella, C.; De Stefano, L.; Rea, I. Synthesis and Surface Modification of Nanostructured F-Doped ZnO: Toward a Transducer for Label-Free Optical Biosensing. *Appl. Sci.* **2019**, *9*, 3380. [[CrossRef](#)]
11. Teymourian, H.; Parrilla, M.; Sempionatto, J.R.; Montiel, N.F.; Barfidokht, A.; Van Echelpoel, R.; De Wael, K.; Wang, J. Wearable Electrochemical Sensors for the Monitoring and Screening of Drugs. *ACS Sens.* **2020**, *5*, 2679–2700. [[CrossRef](#)]
12. Khan, F.A. Nanomaterials: Types, classifications, and sources. *Appl. Nanomater. Hum. Heal.* **2020**, *2*, 1–13. [[CrossRef](#)]
13. Sepúlveda, B.; Angelomé, P.C.; Lechuga, L.M.; Liz-Marzán, L.M. LSPR-based nanobiosensors. *Nano Today* **2009**, *4*, 244–251. [[CrossRef](#)]
14. Mayer, K.M.; Hafner, J.H. Localized surface plasmon resonance sensors. *Chem. Rev.* **2011**, *111*, 3828–3857. [[CrossRef](#)]
15. Ryu, K.R.; Ha, J.W. Influence of shell thickness on the refractive index sensitivity of localized surface plasmon resonance inflection points in silver-coated gold nanorods. *RSC Adv.* **2020**, *10*, 16827–16831. [[CrossRef](#)]
16. Unser, S.; Bruzas, I.; He, J.; Sagle, L. Localized Surface Plasmon Resonance Biosensing: Current Challenges and Approaches. *Sensors* **2015**, *15*, 15684–15716. [[CrossRef](#)]
17. Estevez, M.C.; Otte, M.A.; Sepulveda, B.; Lechuga, L.M. Trends and challenges of refractometric nanoplasmonic biosensors: A review. *Anal. Chim. Acta* **2014**, *806*, 55–73. [[CrossRef](#)]
18. Bhalla, N.; Pan, Y.; Yang, Z.; Payam, A.F. Opportunities and Challenges for Biosensors and Nanoscale Analytical Tools for Pandemics: COVID-19. *ACS Nano* **2020**, *14*, 7783–7807. [[CrossRef](#)]
19. Jung, L.S.; Campbell, C.T.; Chinowsky, T.M.; Mar, M.N.; Yee, S.S. Quantitative Interpretation of the Response of Surface Plasmon Resonance Sensors to Adsorbed Films. *Langmuir* **1998**, *14*, 5636–5648. [[CrossRef](#)]
20. Hammond, J.L.; Bhalla, N.; Rafiee, S.D.; Estrela, P. Localized Surface Plasmon Resonance as a Biosensing Platform for Developing Countries. *Biosensors* **2014**, *4*, 172–188. [[CrossRef](#)]

21. Desiredy, A.; Conn, B.E.; Guo, J.; Yoon, B.; Barnett, R.N.; Monahan, B.M.; Kirschbaum, K.; Griffith, W.P.; Whetten, R.L.; Landman, U.; et al. Ultrastable silver nanoparticles. *Nature* **2013**, *501*, 399–402. [[CrossRef](#)]
22. Qiu, G.; Gai, Z.; Tao, Y.; Schmitt, J.; Kullak-Ublick, G.A.; Wang, J. Dual-Functional Plasmonic Photothermal Biosensors for Highly Accurate Severe Acute Respiratory Syndrome Coronavirus 2 Detection. *ACS Nano* **2020**, *14*, 5268–5277. [[CrossRef](#)] [[PubMed](#)]
23. Iarossi, M.; Schiattarella, C.; Rea, I.; De Stefano, L.; Fittipaldi, R.; Vecchione, A.; Velotta, R.; Ventura, B. Della Colorimetric Immunosensor by Aggregation of Photochemically Functionalized Gold Nanoparticles. *ACS Omega* **2018**, *3*, 3805–3812. [[CrossRef](#)] [[PubMed](#)]
24. Zhao, W.; Brook, M.A.; Li, Y. Design of gold nanoparticle-based colorimetric biosensing assays. *ChemBioChem* **2008**, *9*, 2363–2371. [[CrossRef](#)] [[PubMed](#)]
25. Haes, A.J.; Van Duyne, R.P. A Nanoscale Optical Biosensor: Sensitivity and Selectivity of an Approach Based on the Localized Surface Plasmon Resonance Spectroscopy of Triangular Silver Nanoparticles. *J. Am. Chem. Soc.* **2002**, *124*, 10596–10604. [[CrossRef](#)] [[PubMed](#)]
26. Tahir, M.A.; Dina, N.E.; Cheng, H.; Valev, V.K.; Zhang, L. Surface-enhanced Raman spectroscopy for bioanalysis and diagnosis. *Nanoscale* **2021**, *13*, 11593–11634. [[CrossRef](#)]
27. Suresh, V.; Yap, F.L. Flexible, transparent and robust SERS tapes through a two-step block copolymer self-assembly process. *RSC Adv.* **2015**, *5*, 61671–61677. [[CrossRef](#)]
28. Lakowicz, J.R.; Geddes, C.D.; Gryczynski, I.; Malicka, J.; Gryczynski, Z.; Aslan, K.; Lukomska, J.; Matveeva, E.; Zhang, J.; Badugu, R.; et al. Advances in Surface-Enhanced Fluorescence. *J. Fluoresc.* **2004**, *14*, 425–441. [[CrossRef](#)]
29. Geddes, C.D.; Lakowicz, J.R. Metal-Enhanced Fluorescence concentrating the local field and subsequently increasing. *J. Fluoresc.* **2002**, *12*, 121–129. [[CrossRef](#)]
30. Jeong, Y.; Kook, Y.M.; Lee, K.; Koh, W.G. Metal enhanced fluorescence (MEF) for biosensors: General approaches and a review of recent developments. *Biosens. Bioelectron.* **2018**, *111*, 102–116. [[CrossRef](#)]
31. Stiles, P.L.; Dieringer, J.A.; Shah, N.C.; Van Duyne, R.P. Surface-Enhanced Raman Spectroscopy. *Annu. Rev. Anal. Chem.* **2008**, *1*, 601–626. [[CrossRef](#)] [[PubMed](#)]
32. Jana, D.; Mandal, A.; De, G. High Raman enhancing shape-tunable Ag nanoplates in alumina: A reliable and efficient SERS technique. *ACS Appl. Mater. Interfaces* **2012**, *4*, 3330–3334. [[CrossRef](#)] [[PubMed](#)]
33. Managò, S.; Zito, G.; Rogato, A.; Casalino, M.; Esposito, E.; De Luca, A.C.; De Tommasi, E. Bioderived Three-Dimensional Hierarchical Nanostructures as Efficient Surface-Enhanced Raman Scattering Substrates for Cell Membrane Probing. *ACS Appl. Mater. Interfaces* **2018**, *10*, 12406–12416. [[CrossRef](#)] [[PubMed](#)]
34. Miranda, B.; Chu, K.-Y.; Maffettone, P.L.; Shen, A.Q.; Funari, R. Metal-Enhanced Fluorescence Immunosensor Based on Plasmonic Arrays of Gold Nanoislands on an Etched Glass Substrate. *ACS Appl. Nano Mater.* **2020**, *10*, 10470–10478. [[CrossRef](#)]
35. Minopoli, A.; Della Ventura, B.; Lenyk, B.; Gentile, F.; Tanner, J.A.; Offenhäusser, A.; Mayer, D.; Velotta, R. Ultrasensitive antibody-aptamer plasmonic biosensor for malaria biomarker detection in whole blood. *Nat. Commun.* **2020**, *11*, 1–10. [[CrossRef](#)]
36. Miranda, B.; Moretta, R.; Dardano, P.; Rea, I.; Forestiere, C.; Stefano, L. De H3 (Hydrogel-Based, High-Sensitivity, Hybrid) Plasmonic Transducers for Biomolecular Interactions Monitoring. *Adv. Mater. Technol.* **2022**, *4*, 2101425. [[CrossRef](#)]
37. Dos Santos, P.S.S.; de Almeida, J.M.M.M.; Pastoriza-santos, I.; Coelho, L.C.C. Advances in Plasmonic Sensing at the NIR—A Review. *Sensors* **2021**, *21*, 2111. [[CrossRef](#)]
38. Teo, B.K.; Sun, X.H. From top-down to bottom-up to hybrid nanotechnologies: Road to nanodevices. *J. Clust. Sci.* **2006**, *17*, 529–540. [[CrossRef](#)]
39. Lin, X.; Hasi, W.L.J.; Han, S.Q.G.W.; Lou, X.T.; Lin, D.Y.; Lu, Z.W. Fabrication of transparent SERS platform via interface self-assembly of gold nanorods and gel trapping technique for on-site real time detection. *Phys. Chem. Chem. Phys.* **2015**, *17*, 31324–31331. [[CrossRef](#)]
40. Iqbal, P.; Preece, J.A.; Mendes, P.M. Nanotechnology: The “Top-Down” and “Bottom-Up” Approaches. In *Supramolecular Chemistry*; John Wiley & Sons, Ltd.: Chichester, UK, 2012.
41. Pastoriza-Santos, I.; Kinnear, C.; Pérez-Juste, J.; Mulvaney, P.; Liz-Marzán, L.M. Plasmonic polymer nanocomposites. *Nat. Rev. Mater.* **2018**, *3*, 375–391. [[CrossRef](#)]
42. Kermanshahian, K.; Yadegar, A.; Ghourchian, H. Gold nanorods etching as a powerful signaling process for plasmonic multicolorimetric chemo-/biosensors: Strategies and applications. *Coord. Chem. Rev.* **2021**, *442*, 213934. [[CrossRef](#)]
43. Orendorff, C.J.; Sau, T.K.; Murphy, C.J. Shape-Dependent Plasmon-Resonant Gold Nanoparticles. *Small* **2006**, *2*, 636–639. [[CrossRef](#)] [[PubMed](#)]
44. Nehl, C.L.; Hafner, J.H. Shape-dependent plasmon resonances of gold nanoparticles. *J. Mater. Chem.* **2008**, *18*, 2415–2419. [[CrossRef](#)]
45. Mock, J.J.; Smith, D.R.; Schultz, S. Local Refractive Index Dependence of Plasmon Resonance Spectra from Individual Nanoparticles. *Nano Lett.* **2003**, *3*, 485–491. [[CrossRef](#)]
46. Sun, Y.; Xia, Y. Increased Sensitivity of Surface Plasmon Resonance of Gold Nanoshells Compared to That of Gold Solid Colloids in Response to Environmental Changes. *Anal. Chem.* **2002**, *74*, 5297–5305. [[CrossRef](#)] [[PubMed](#)]
47. Link, S.; El-Sayed, M.A. Size and Temperature Dependence of the Plasmon Absorption of Colloidal Gold Nanoparticles. *J. Phys. Chem. B* **1999**, *103*, 4212–4217. [[CrossRef](#)]

48. Chen, H.; Kou, X.; Yang, Z.; Ni, W.; Wang, J. Shape- and Size-Dependent Refractive Index Sensitivity of Gold Nanoparticles. *Langmuir* **2008**, *24*, 5233–5237. [[CrossRef](#)]
49. Sherry, L.J.; Chang, S.-H.; Schatz, G.C.; Van Duyne, R.P.; Wiley, B.J.; Xia, Y. Localized Surface Plasmon Resonance Spectroscopy of Single Silver Nanocubes. *Nano Lett.* **2005**, *5*, 2034–2038. [[CrossRef](#)]
50. Mahani, M.; Alimohamadi, F.; Torkzadeh-Mahani, M.; Hassani, Z.; Khakbaz, F.; Divsar, F.; Yoosefian, M. LSPR biosensing for the early-stage prostate cancer detection using hydrogen bonds between PSA and antibody: Molecular dynamic and experimental study. *J. Mol. Liq.* **2021**, *324*, 114736. [[CrossRef](#)]
51. Besselink, G.A.J.; Kooyman, R.P.H.; Van Os, P.J.H.J.; Engbers, G.H.M.; Schasfoort, R.B.M. Signal amplification on planar and gel-type sensor surfaces in surface plasmon resonance-based detection of prostate-specific antigen. *Anal. Biochem.* **2004**, *333*, 165–173. [[CrossRef](#)]
52. Della Ventura, B.; Schiavo, L.; Altucci, C.; Esposito, R.; Velotta, R. Light assisted antibody immobilization for bio-sensing. *Biomed. Opt. Express* **2011**, *2*, 3223–3231. [[CrossRef](#)] [[PubMed](#)]
53. Funari, R.; Della Ventura, B.; Altucci, C.; Offenhäusser, A.; Mayer, D.; Velotta, R. Single Molecule Characterization of UV-Activated Antibodies on Gold by Atomic Force Microscopy. *Langmuir* **2016**, *32*, 8084–8091. [[CrossRef](#)] [[PubMed](#)]
54. Gao, Y.; Wu, Y.; Di, J. Colorimetric detection of glucose based on gold nanoparticles coupled with silver nanoparticles. *Spectrochim. Acta Part A Mol. Biomol. Spectrosc.* **2017**, *173*, 207–212. [[CrossRef](#)]
55. Politi, J.; De Stefano, L.; Rea, I.; Gravagnuolo, A.M.; Giardina, P.; Methivier, C.; Casale, S.; Spadavecchia, J. One-pot synthesis of a gold nanoparticle-Vmh2 hydrophobin nanobiocomplex for glucose monitoring. *Nanotechnology* **2016**, *27*, 195701. [[CrossRef](#)]
56. Spadavecchia, J.; Perumal, R.; Casale, S.; Krafft, J.-M.; Methivier, C.; Pradier, C.-M. Polyethylene glycol gold-nanoparticles: Facile nanostructuring of doxorubicin and its complex with DNA molecules for SERS detection. *Chem. Phys. Lett.* **2016**, *648*, 182–188. [[CrossRef](#)]
57. Politi, J.; De Stefano, L.; Longobardi, S.; Giardina, P.; Rea, I.; Methivier, C.; Pradier, C.-M.; Casale, S.; Spadavecchia, J. The amphiphilic hydrophobin Vmh2 plays a key role in one step synthesis of hybrid protein–gold nanoparticles. *Colloids Surf. B Biointerfaces* **2015**, *136*, 214–221. [[CrossRef](#)] [[PubMed](#)]
58. Lee, J.-H.; Cho, H.-Y.; Choi, H.K.; Lee, J.-Y.; Choi, J.-W. Application of Gold Nanoparticle to Plasmonic Biosensors. *Int. J. Mol. Sci.* **2018**, *19*, 2021. [[CrossRef](#)]
59. Guo, Y.; Wu, J.; Li, J.; Ju, H. A plasmonic colorimetric strategy for biosensing through enzyme guided growth of silver nanoparticles on gold nanostars. *Biosens. Bioelectron.* **2016**, *78*, 267–273. [[CrossRef](#)]
60. Faridfar, G.; Zeinoddini, M.; Akbarzedehtkolahi, S.; Faridfar, S.; Nemati, A.S. Immunodiagnostic of *Vibrio cholerae* O1 using localized surface plasmon resonance (LSPR) biosensor. *Int. Microbiol.* **2021**, *24*, 115–122. [[CrossRef](#)]
61. Tramontano, C.; Miranda, B.; Chianese, G.; De Stefano, L.; Forestiere, C.; Pirozzi, M.; Rea, I. Design of gelatin-capped plasmonic-diatomite nanoparticles with enhanced galunisertib loading capacity for drug delivery applications. *Int. J. Mol. Sci.* **2021**, *22*, 10755. [[CrossRef](#)]
62. Lee, T.; Kim, G.H.; Kim, S.M.; Hong, K.; Kim, Y.; Park, C.; Sohn, H.; Min, J. Label-free localized surface plasmon resonance biosensor composed of multi-functional DNA 3 way junction on hollow Au spike-like nanoparticles (HAuSN) for avian influenza virus detection. *Colloids Surf. B Biointerfaces* **2019**, *182*, 110341. [[CrossRef](#)] [[PubMed](#)]
63. Li, Z.; Yi, Y.; Luo, X.; Xiong, N.; Liu, Y.; Li, S.; Sun, R.; Wang, Y.; Hu, B.; Chen, W.; et al. Development and clinical application of a rapid IgM-IgG combined antibody test for SARS-CoV-2 infection diagnosis. *J. Med. Virol.* **2020**, *92*, 1518–1524. [[CrossRef](#)] [[PubMed](#)]
64. Moitra, P.; Alafeef, M.; Dighe, K.; Frieman, M.B.; Pan, D. Selective Naked-Eye Detection of SARS-CoV-2 Mediated by N Gene Targeted Antisense Oligonucleotide Capped Plasmonic Nanoparticles. *ACS Nano* **2020**, *14*, 7617–7627. [[CrossRef](#)]
65. Karakuş, E.; Erdemir, E.; Demirbilek, N.; Liv, L. Colorimetric and electrochemical detection of SARS-CoV-2 spike antigen with a gold nanoparticle-based biosensor. *Anal. Chim. Acta* **2021**, *1182*, 338939. [[CrossRef](#)]
66. Sheth, S.; Barnard, E.; Hyatt, B.; Rathinam, M.; Zustiak, S.P. Predicting Drug Release From Degradable Hydrogels Using Fluorescence Correlation Spectroscopy and Mathematical Modeling. *Front. Bioeng. Biotechnol.* **2019**, *7*, 410. [[CrossRef](#)] [[PubMed](#)]
67. Zhang, C.; Rodriguez, E.; Bi, C.; Zheng, X.; Suresh, D.; Suh, K.; Li, Z.; Elsebaei, F.; Hage, D.S. High performance affinity chromatography and related separation methods for the analysis of biological and pharmaceutical agents. *Analyst* **2018**, *143*, 374–391. [[CrossRef](#)]
68. Zheng, F.; Xiong, W.; Sun, S.; Zhang, P.; Zhu, J.J. Recent advances in drug release monitoring. *Nanophotonics* **2019**, *8*, 391–413. [[CrossRef](#)]
69. Okabe, K.; Inada, N.; Gota, C.; Harada, Y.; Funatsu, T.; Uchiyama, S. Intracellular temperature mapping with a fluorescent polymeric thermometer and fluorescence lifetime imaging microscopy. *Nat. Commun.* **2012**, *3*, 705. [[CrossRef](#)]
70. Qiu, F.; Wang, D.; Zhu, Q.; Zhu, L.; Tong, G.; Lu, Y.; Yan, D.; Zhu, X. Real-time monitoring of anticancer drug release with highly fluorescent star-conjugated copolymer as a drug carrier. *Biomacromolecules* **2014**, *15*, 1355–1364. [[CrossRef](#)]
71. Tian, F.; Conde, J.; Bao, C.; Chen, Y.; Curtin, J.; Cui, D. Gold nanostars for efficient in vitro and in vivo real-time SERS detection and drug delivery via plasmonic-tunable Raman/FTIR imaging. *Biomaterials* **2016**, *106*, 87–97. [[CrossRef](#)]
72. Montgomery, J.M.; Imre, A.; Welp, U.; Vlasko-Vlasov, V.; Gray, S.K.; Ghaemi, H.F.; Thio, T.; Grupp, D.E.; Ebbesen, T.W. SERS enhancements via periodic arrays of gold nanoparticles on silver film structures. *Opt. Express* **2009**, *17*, 8669–8675. [[CrossRef](#)] [[PubMed](#)]

73. Terracciano, M.; Napolitano, M.; De Stefano, L.; De Luca, A.C.; Rea, I. Gold decorated porous biosilica nanodevices for advanced medicine. *Nanotechnology* **2018**, *29*, 235601. [[CrossRef](#)] [[PubMed](#)]
74. Lai, C.H.; Wang, G.A.; Ling, T.K.; Wang, T.J.; Chiu, P.K.; Chou Chau, Y.F.; Huang, C.C.; Chiang, H.P. Near infrared surface-enhanced Raman scattering based on star-shaped gold/silver nanoparticles and hyperbolic metamaterial. *Sci. Rep.* **2017**, *7*, 5446. [[CrossRef](#)] [[PubMed](#)]
75. Managò, S.; Tramontano, C.; Cave, D.D.; Chianese, G.; Zito, G.; De Stefano, L.; Terracciano, M.; Lonardo, E.; De Luca, A.C.; Rea, I.; et al. SERS quantification of Galunisertib delivery in colorectal cancer cells by plasmonic-assisted diatomite nanoparticles. *Small* **2021**, *17*, 2101711. [[CrossRef](#)]
76. Reifarth, M.; Hoepfener, S.; Schubert, U.S. Uptake and Intracellular Fate of Engineered Nanoparticles in Mammalian Cells: Capabilities and Limitations of Transmission Electron Microscopy—Polymer-Based Nanoparticles. *Adv. Mater.* **2018**, *30*, 1703704. [[CrossRef](#)]
77. Li, L.; Tang, B.; Li, X.; Duan, X.; Yang, P. Accurate in situ monitoring of mitochondrial H₂O₂ by robust SERS nanoprobe with a Au–Se interface. *Anal. Chem.* **2021**, *93*, 4059–4065. [[CrossRef](#)]
78. Yücel, G.; Zhao, Z.; El-Battrawy, I.; Lan, H.; Lang, S.; Li, X.; Buljubasic, F.; Zimmermann, W.H.; Cyganek, L.; Utikal, J.; et al. Lipopolysaccharides induced inflammatory responses and electrophysiological dysfunctions in human-induced pluripotent stem cell derived cardiomyocytes. *Sci. Rep.* **2017**, *7*, 2935. [[CrossRef](#)]
79. Li, Y.; Italiani, P.; Casals, E.; Tran, N.; Puentes, V.F.; Boraschi, D. Optimising the use of commercial LAL assays for the analysis of endotoxin contamination in metal colloids and metal oxide nanoparticles. *Nanotoxicology* **2015**, *9*, 462–473. [[CrossRef](#)]
80. Verde, A.; Mangini, M.; Managò, S.; Tramontano, C.; Rea, I.; Boraschi, D.; Italiani, P.; De Luca, A.C. SERS Sensing of Bacterial Endotoxin on Gold Nanoparticles. *Front. Immunol.* **2021**, *12*, 758410. [[CrossRef](#)]
81. Hu, W.; Xia, L.; Hu, Y.; Li, G. Recent progress on three-dimensional substrates for surface-enhanced Raman spectroscopic analysis. *Microchem. J.* **2022**, *172*, 106908. [[CrossRef](#)]
82. Han, Y.; Wu, S.R.; Tian, X.D.; Zhang, Y. Optimizing the SERS Performance of 3D Substrates through Tunable 3D Plasmonic Coupling toward Label-Free Liver Cancer Cell Classification. *ACS Appl. Mater. Interfaces* **2020**, *12*, 28965–28974. [[CrossRef](#)] [[PubMed](#)]
83. Kolle, M. *Photonic Structures Inspired by Nature*; Springer: Berlin/Heidelberg, Germany, 2011.
84. Pannico, M.; Rea, I.; Chandrasekaran, S.; Musto, P.; Voelcker, N.H.; De Stefano, L. Electroless Gold-Modified Diatoms as Surface-Enhanced Raman Scattering Supports. *Nanoscale Res. Lett.* **2016**, *11*, 315. [[CrossRef](#)] [[PubMed](#)]
85. De Angelis, F.; Malerba, M.; Patrini, M.; Miele, E.; Das, G.; Toma, A.; Zaccaria, R.P.; Di Fabrizio, E. 3D hollow nanostructures as building blocks for multifunctional plasmonics. *Nano Lett.* **2013**, *13*, 3553–3558. [[CrossRef](#)] [[PubMed](#)]
86. Andreou, C.; Neuschmelting, V.; Tschaharganeh, D.F.; Huang, C.H.; Oseledchyk, A.; Iacono, P.; Karabeber, H.; Colen, R.R.; Mannelli, L.; Lowe, S.W.; et al. Imaging of Liver Tumors Using Surface-Enhanced Raman Scattering Nanoparticles. *ACS Nano* **2016**, *10*, 5015–5026. [[CrossRef](#)]
87. Mir-Simon, B.; Reche-Perez, I.; Guerrini, L.; Pazos-Perez, N.; Alvarez-Puebla, R.A. Universal one-pot and scalable synthesis of SERS encoded nanoparticles. *Chem. Mater.* **2015**, *27*, 950–958. [[CrossRef](#)]
88. Oseledchyk, A.; Andreou, C.; Wall, M.A.; Kircher, M.F. Folate-Targeted Surface-Enhanced Resonance Raman Scattering Nanoprobe Ratiometry for Detection of Microscopic Ovarian Cancer. *ACS Nano* **2017**, *11*, 1488–1497. [[CrossRef](#)] [[PubMed](#)]
89. Pazos-Perez, N.; Fitzgerald, J.M.; Giannini, V.; Guerrini, L.; Alvarez-Puebla, R.A. Modular assembly of plasmonic core–satellite structures as highly brilliant SERS-encoded nanoparticles. *Nanoscale Adv.* **2019**, *1*, 122–131. [[CrossRef](#)]
90. Mallia, R.J.; McVeigh, P.Z.; Fisher, C.J.; Veilleux, I.; Wilson, B.C. Wide-field multiplexed imaging of EGFR-targeted cancers using topical application of NIR SERS nanoprobe. *Nanomedicine* **2014**, *10*, 89–101. [[CrossRef](#)]
91. Nicolson, F.; Andreiuk, B.; Andreou, C.; Hsu, H.T.; Rudder, S.; Kircher, M.F. Non-invasive in vivo imaging of cancer using Surface-Enhanced spatially offset raman spectroscopy (SEORS). *Theranostics* **2019**, *9*, 5899–5913. [[CrossRef](#)]
92. Wen, Y.; Truong, V.X.; Li, M. Real-Time Intraoperative Surface-Enhanced Raman Spectroscopy-Guided Thermosurgical Eradication of Residual Microtumors in Orthotopic Breast Cancer. *Nano Lett.* **2021**, *21*, 3066–3074. [[CrossRef](#)]
93. Wang, Q.; Wang, L. Lab-on-fiber: Plasmonic nano-arrays for sensing. *Nanoscale* **2020**, *12*, 7485–7499. [[CrossRef](#)] [[PubMed](#)]
94. Levin, A.D.; Ringaci, A.; Alenichev, M.K.; Drozhzhennikova, E.B.; Shevchenko, K.G.; Cherkasov, V.R.; Nikitin, M.P.; Nikitin, P.I. Dynamic light scattering biosensing based on analyte-induced inhibition of nanoparticle aggregation. *Anal. Bioanal. Chem.* **2020**, *412*, 3423–3431. [[CrossRef](#)] [[PubMed](#)]
95. Hu, S.; Huang, P.-J.J.; Wang, J.; Liu, J. Dissecting the Effect of Salt for More Sensitive Label-Free Colorimetric Detection of DNA Using Gold Nanoparticles. *Anal. Chem.* **2020**, *92*, 13354–13360. [[CrossRef](#)]
96. Aryal, S.; Remant, R.B.; Bhattarai, N.; Kim, C.K.; Kim, H.Y. Study of electrolyte induced aggregation of gold nanoparticles capped by amino acids. *J. Colloid Interface Sci.* **2006**, *299*, 191–197. [[CrossRef](#)]
97. Guo, R.; Hakala, T.K.; Törmä, P. Geometry dependence of surface lattice resonances in plasmonic nanoparticle arrays. *Phys. Rev. B* **2017**, *95*, 155423. [[CrossRef](#)]
98. Bhalla, N.; Sathish, S.; Sinha, A.; Shen, A.Q. Biosensors: Large-Scale Nanophotonic Structures for Long-Term Monitoring of Cell Proliferation (Adv. Biosys. 4/2018). *Adv. Biosyst.* **2018**, *2*, 1870031. [[CrossRef](#)]
99. Im, H.; Lee, S.H.; Wittenberg, N.J.; Johnson, T.W.; Lindquist, N.C.; Nagpal, P.; Norris, D.J.; Oh, S.H. Template-stripped smooth Ag nanohole arrays with silica shells for surface plasmon resonance biosensing. *ACS Nano* **2011**, *5*, 6244–6253. [[CrossRef](#)]

100. Jeon, H.C.; Heo, C.J.; Lee, S.Y.; Yang, S.M. Hierarchically Ordered Arrays of Noncircular Silicon Nanowires Featured by Holographic Lithography Toward a High-Fidelity Sensing Platform. *Adv. Funct. Mater.* **2012**, *22*, 4268–4274. [[CrossRef](#)]
101. Menezes, J.W.; Ferreira, J.; Santos, M.J.L.; Cescato, L.; Brolo, A.G. Large-Area Fabrication of Periodic Arrays of Nanoholes in Metal Films and Their Application in Biosensing and Plasmonic-Enhanced Photovoltaics. *Adv. Funct. Mater.* **2010**, *20*, 3918–3924. [[CrossRef](#)]
102. Kim, D.M.; Park, J.S.; Jung, S.W.; Yeom, J.; Yoo, S.M. Biosensing Applications Using Nanostructure-Based Localized Surface Plasmon Resonance Sensors. *Sensors* **2021**, *21*, 3191. [[CrossRef](#)]
103. Asgari, S.; Sun, L.; Lin, J.; Weng, Z.; Wu, G.; Zhang, Y.; Lin, M. Nanofibrillar cellulose/Au@Ag nanoparticle nanocomposite as a SERS substrate for detection of paraquat and thiram in lettuce. *Microchim. Acta* **2020**, *187*, 390. [[CrossRef](#)] [[PubMed](#)]
104. Bhalla, N.; Jamshaid, A.; Leung, M.H.M.; Ishizu, N.; Shen, A.Q. Electrical contact of metals at the nanoscale overcomes the oxidative susceptibility of silver-based nanobiosensors. *ACS Appl. Nano Mater.* **2019**, *2*, 2064–2075. [[CrossRef](#)]
105. Ren, S.; Zhang, Z.; Xu, C.; Guo, L.; Lu, R.; Sun, Y.; Guo, J.; Qin, R.; Qin, W.; Gu, J. Distribution of IgG galactosylation as a promising biomarker for cancer screening in multiple cancer types. *Cell Res.* **2016**, *26*, 963–966. [[CrossRef](#)] [[PubMed](#)]
106. Vestri, A.; Rippa, M.; Marchesano, V.; Sagnelli, D.; Margheri, G.; Zhou, J.; Petti, L. LSPR immuno-sensing based on iso-Y nanopillars for highly sensitive and specific imidacloprid detection. *J. Mater. Chem. B* **2021**, *9*, 9153–9161. [[CrossRef](#)] [[PubMed](#)]
107. Chen, J.S.; Chen, P.F.; Lin, H.T.H.; Huang, N.T. A Localized surface plasmon resonance (LSPR) sensor integrated automated microfluidic system for multiplex inflammatory biomarker detection. *Analyst* **2020**, *145*, 7654–7661. [[CrossRef](#)] [[PubMed](#)]
108. Khan, Y.; Li, A.; Chang, L.; Li, L.; Guo, L. Gold nano disks arrays for localized surface plasmon resonance based detection of PSA cancer marker. *Sens. Actuators B Chem.* **2018**, *255*, 1298–1307. [[CrossRef](#)]
109. Terracciano, M.; Rea, I.; Borbone, N.; Moretta, R.; Oliviero, G.; Piccialli, G.; De Stefano, L. Porous silicon-based aptasensors: The next generation of label-free devices for health monitoring. *Molecules* **2019**, *24*, 2216. [[CrossRef](#)]
110. Taghavi, A.; Rahbarizadeh, F.; Abbasian, S.; Moshaii, A. Label-Free LSPR Prostate-Specific Antigen Immune-Sensor Based on GLAD-Fabricated Silver Nano-columns. *Plasmonics* **2020**, *15*, 753–760. [[CrossRef](#)]
111. Vieth, R. Vitamin D Toxicity, Policy, and Science. *J. Bone Miner. Res.* **2007**, *22*, V64–V68. [[CrossRef](#)]
112. Jo, S.; Lee, W.; Park, J.; Park, H.; Kim, M.; Kim, W.; Hong, J.; Park, J. Wide-range direct detection of 25-hydroxyvitamin D3 using polyethylene-glycol-free gold nanorod based on LSPR aptasensor. *Biosens. Bioelectron.* **2021**, *181*, 956–5663. [[CrossRef](#)]
113. Kim, J.; Oh, S.Y.; Shukla, S.; Hong, S.B.; Heo, N.S.; Bajpai, V.K.; Chun, H.S.; Jo, C.-H.; Choi, B.G.; Huh, Y.S.; et al. Heteroassembled gold nanoparticles with sandwich-immunoassay LSPR chip format for rapid and sensitive detection of hepatitis B virus surface antigen (HBsAg). *Biosens. Bioelectron.* **2018**, *107*, 118–122. [[CrossRef](#)] [[PubMed](#)]
114. Bastús, N.G.; Comenge, J.; Puentes, V. Kinetically controlled seeded growth synthesis of citrate-stabilized gold nanoparticles of up to 200 nm: Size focusing versus ostwald ripening. *Langmuir* **2011**, *27*, 11098–11105. [[CrossRef](#)] [[PubMed](#)]
115. Funari, R.; Chu, K.Y.; Shen, A.Q. Detection of antibodies against SARS-CoV-2 spike protein by gold nanopikes in an opto-microfluidic chip. *Biosens. Bioelectron.* **2020**, *169*, 112578. [[CrossRef](#)] [[PubMed](#)]
116. Focsan, M.; Campu, A.; Craciun, A.M.; Potara, M.; Leordean, C.; Maniu, D.; Astilean, S. A simple and efficient design to improve the detection of biotin-streptavidin interaction with plasmonic nanobiosensors. *Biosens. Bioelectron.* **2016**, *86*, 728–735. [[CrossRef](#)]
117. Pilot, R.; Signorini, R.; Durante, C.; Orian, L.; Bhamidipati, M.; Fabris, L. A Review on Surface-Enhanced Raman Scattering. *Biosensors* **2019**, *9*, 57. [[CrossRef](#)]
118. Langer, J.; de Aberasturi, D.J.; Aizpurua, J.; Alvarez-Puebla, R.A.; Auguie, B.; Baumberg, J.J.; Bazan, G.C.; Bell, S.E.J.; Boisen, A.; Brolo, A.G.; et al. Present and future of surface-enhanced Raman scattering. *ACS Nano* **2020**, *14*, 28–117. [[CrossRef](#)]
119. Muhammad, M.; Shao, C.-S.; Huang, Q. Aptamer-functionalized Au nanoparticles array as the effective SERS biosensor for label-free detection of interleukin-6 in serum. *Sens. Actuators B Chem.* **2021**, *334*, 129607. [[CrossRef](#)]
120. Kang, T.; Zhu, J.; Luo, X.; Jia, W.; Wu, P.; Cai, C. Controlled Self-Assembly of a Close-Packed Gold Octahedra Array for SERS Sensing Exosomal MicroRNAs. *Anal. Chem.* **2021**, *93*, 2519–2526. [[CrossRef](#)]
121. Mei, Z.; Tang, L. Surface-Plasmon-Coupled Fluorescence Enhancement Based on Ordered Gold Nanorod Array Biochip for Ultrasensitive DNA Analysis. *Anal. Chem.* **2017**, *89*, 633–639. [[CrossRef](#)]
122. Chen, H.; Park, S.G.; Choi, N.; Moon, J.I.; Dang, H.; Das, A.; Lee, S.; Kim, D.G.; Chen, L.; Choo, J. SERS imaging-based aptasensor for ultrasensitive and reproducible detection of influenza virus A. *Biosens. Bioelectron.* **2020**, *167*, 112496. [[CrossRef](#)]
123. Badshah, M.A.; Koh, N.Y.; Zia, A.W.; Abbas, N.; Zahra, Z.; Saleem, M.W. Recent Developments in Plasmonic Nanostructures for Metal Enhanced Fluorescence-Based Biosensing. *Nanomaterials* **2020**, *10*, 1749. [[CrossRef](#)] [[PubMed](#)]
124. Laupland, K.B.; Gregson, D.B.; Zygun, D.A.; Doig, C.J.; Mortis, G.; Church, D.L. Severe bloodstream infections: A population-based assessment. *Crit. Care Med.* **2004**, *32*, 992–997. [[CrossRef](#)] [[PubMed](#)]
125. Kumar, A.; Roberts, D.; Wood, K.E.; Light, B.; Parrillo, J.E.; Sharma, S.; Suppes, R.; Feinstein, D.; Zanotti, S.; Taiberg, L.; et al. Duration of hypotension before initiation of effective antimicrobial therapy is the critical determinant of survival in human septic shock. *Crit. Care Med.* **2006**, *34*, 1589–1596. [[CrossRef](#)] [[PubMed](#)]
126. Martin, G.S. Sepsis, severe sepsis and septic shock: Changes in incidence, pathogens and outcomes. *Expert Rev. Anti. Infect. Ther.* **2012**, *10*, 701–706. [[CrossRef](#)]
127. Sun, L.L.; Leo, Y.S.; Zhou, X.; Ng, W.; Wong, T.I.; Deng, J. Localized surface plasmon resonance based point-of-care system for sepsis diagnosis. *Mater. Sci. Energy Technol.* **2020**, *3*, 274–281. [[CrossRef](#)]

128. Avolio, R.; Gentile, G.; Avella, M.; Carfagna, C.; Errico, M.E. Polymer–filler interactions in PET/CaCO₃ nanocomposites: Chain ordering at the interface and physical properties. *Eur. Polym. J.* **2013**, *49*, 419–427. [[CrossRef](#)]
129. Li, L.; Chin, W.S. Rapid Fabrication of a Flexible and Transparent Ag Nanocubes@PDMS Film as a SERS Substrate with High Performance. *ACS Appl. Mater. Interfaces* **2020**, *12*, 37538–37548. [[CrossRef](#)]
130. Shiohara, A.; Langer, J.; Polavarapu, L.; Liz-Marzán, L.M. Solution processed polydimethylsiloxane/gold nanostar flexible substrates for plasmonic sensing. *Nanoscale* **2014**, *6*, 9817–9823. [[CrossRef](#)]
131. Yang, N.; You, T.T.; Gao, Y.K.; Zhang, C.M.; Yin, P.G. Rapid fabrication of flexible and transparent gold nanorods/poly (methyl methacrylate) membrane substrate for SERS nanosensor application. *Spectrochim. Acta - Part A Mol. Biomol. Spectrosc.* **2018**, *202*, 376–381. [[CrossRef](#)]
132. Zuo, Z.; Zhu, K.; Gu, C.; Wen, Y.; Cui, G.; Qu, J. Transparent, flexible surface enhanced Raman scattering substrates based on Ag-coated structured PET (polyethylene terephthalate) for in-situ detection. *Appl. Surf. Sci.* **2016**, *379*, 66–72. [[CrossRef](#)]
133. Zhang, C.L.; Cao, F.H.; Wang, J.L.; Yu, Z.L.; Ge, J.; Lu, Y.; Wang, Z.H.; Yu, S.H. Highly Stimuli-Responsive Au Nanorods/Poly(N-isopropylacrylamide) (PNIPAM) Composite Hydrogel for Smart Switch. *ACS Appl. Mater. Interfaces* **2017**, *9*, 24857–24863. [[CrossRef](#)] [[PubMed](#)]
134. Shir, D.; Ballard, Z.S.; Ozcan, A. Flexible Plasmonic Sensors. *IEEE J. Sel. Top. Quantum Electron.* **2016**, *22*, 12–20. [[CrossRef](#)] [[PubMed](#)]
135. Kameche, F.; Heni, W.; Telitel, S.; Ge, D.; Vidal, L.; Dumur, F.; Gigmes, D.; Lalevée, J.; Marguet, S.; Douillard, L.; et al. Plasmon-triggered living photopolymerization for elaboration of hybrid polymer/metal nanoparticles. *Mater. Today* **2020**, *40*, 38–47. [[CrossRef](#)]
136. Polavarapu, L.; Liz-Marzán, L.M. Towards low-cost flexible substrates for nanoplasmonic sensing. *Phys. Chem. Chem. Phys.* **2013**, *15*, 5288–5300. [[CrossRef](#)] [[PubMed](#)]
137. Jiang, C.; Qian, Y.; Gao, Q.; Dong, J.; Qian, W. In Situ controllable preparation of gold nanorods in thermo-responsive hydrogels and their application in surface enhanced Raman scattering. *J. Mater. Chem.* **2010**, *20*, 8711–8716. [[CrossRef](#)]
138. Herrmann, A.; Haag, R.; Schedler, U. Hydrogels and Their Role in Biosensing Applications. *Adv. Healthc. Mater.* **2021**, *10*, 1–25. [[CrossRef](#)]
139. Chen, G.; Tang, W.; Wang, X.; Zhao, X.; Chen, C.; Zhu, Z. Applications of Hydrogels with Special Physical Properties in Biomedicine. *Polymers* **2019**, *11*, 1420. [[CrossRef](#)]
140. Liu, Y.; Cheong NG, S.; Yu, J.; Tsai, W.B. Modification and crosslinking of gelatin-based biomaterials as tissue adhesives. *Colloids Surf. B Biointerfaces* **2019**, *174*, 316–323. [[CrossRef](#)]
141. Xue, K.; Wang, X.; Yong, P.W.; Young, D.J.; Wu, Y.L.; Li, Z.; Loh, X.J. Hydrogels as Emerging Materials for Translational Biomedicine. *Adv. Ther.* **2019**, *2*, 1800088. [[CrossRef](#)]
142. Buenger, D.; Topuz, F.; Groll, J. Hydrogels in sensing applications. *Prog. Polym. Sci.* **2012**, *37*, 1678–1719. [[CrossRef](#)]
143. Feng, L.; Wang, L.; Hu, Z.; Tian, Y.; Xian, Y.; Jin, L. Encapsulation of horseradish peroxidase into hydrogel, and its bioelectrochemistry. *Microchim. Acta* **2009**, *164*, 49–54. [[CrossRef](#)]
144. Wang, Z.; Liu, Y.; Wang, Z.; Huang, X.; Huang, W. Hydrogel-based composites: Unlimited platforms for biosensors and diagnostics. *View* **2021**, 20200165. [[CrossRef](#)]
145. Choe, A.; Yeom, J.; Shanker, R.; Kim, M.P.; Kang, S.; Ko, H. Stretchable and wearable colorimetric patches based on thermoresponsive plasmonic microgels embedded in a hydrogel film. *NPG Asia Mater.* **2018**, *10*, 912–922. [[CrossRef](#)]
146. Heilmann, A. *Polymer Films with Embedded Metal Nanoparticles*; Springer Science & Business Media: Berlin, Germany, 2003; p. 52. [[CrossRef](#)]
147. Willner, I. Stimuli-Controlled Hydrogels and Their Applications. *Acc. Chem. Res.* **2017**, *50*, 657–658. [[CrossRef](#)] [[PubMed](#)]
148. Caliò, A.; Rea, I.; Rendina, I.; Politi, J.; De Stefano, L.; Dardano, P. Optically monitored drug delivery patch based on porous silicon and polymer microneedles. *Biomed. Opt. Express* **2016**, *7*, 1645–1655. [[CrossRef](#)]
149. Battisti, M.; De Martino, S.; Miranda, B.; Tammara, C.; Dardano, P.; Dello Iacono, S.; Luca, A.; Stefano, D.E. Oxygen indicator films of acrylate photopolymers and TiO₂ nanoparticles with tunable response times. *Opt. Mater. Express* **2021**, *11*, 2244. [[CrossRef](#)]
150. Montelongo, Y.; Yetisen, A.K.; Butt, H.; Yun, S.H. Reconfigurable optical assembly of nanostructures. *Nat. Commun.* **2016**, *7*, 12002. [[CrossRef](#)]
151. Lv, S.W.; Liu, Y.; Xie, M.; Wang, J.; Yan, X.W.; Li, Z.; Dong, W.G.; Huang, W.H. Near-Infrared Light-Responsive Hydrogel for Specific Recognition and Photothermal Site-Release of Circulating Tumor Cells. *ACS Nano* **2016**, *10*, 6201–6210. [[CrossRef](#)]
152. Xing, R.; Liu, K.; Jiao, T.; Zhang, N.; Ma, K.; Zhang, R.; Zou, Q.; Ma, G.; Yan, X.; Xing, R.; et al. An Injectable Self-Assembling Collagen–Gold Hybrid Hydrogel for Combinatorial Antitumor Photothermal/Photodynamic Therapy. *Adv. Mater.* **2016**, *28*, 3669–3676. [[CrossRef](#)]
153. Sershen, S.R.; Mensing, G.A.; Ng, M.; Halas, N.J.; Beebe, D.J.; West, J.L. Independent Optical Control of Microfluidic Valves Formed from Optomechanically Responsive Nanocomposite Hydrogels. *Adv. Mater.* **2005**, *17*, 1366–1368. [[CrossRef](#)]
154. Zhou, Y.; Hauser, A.W.; Bende, N.P.; Kuzyk, M.G.; Hayward, R.C. Waveguiding Microactuators Based on a Photothermally Responsive Nanocomposite Hydrogel. *Adv. Funct. Mater.* **2016**, *26*, 5447–5452. [[CrossRef](#)]
155. Shi, Q.; Xia, H.; Li, P.; Wang, Y.-S.; Wang, L.; Li, S.-X.; Wang, G.; Lv, C.; Niu, L.-G.; Sun, H.-B.; et al. Photothermal Surface Plasmon Resonance and Interband Transition-Enhanced Nanocomposite Hydrogel Actuators with Hand-Like Dynamic Manipulation. *Adv. Opt. Mater.* **2017**, *5*, 1700442. [[CrossRef](#)]

156. Schild, H.G. Poly(N-isopropylacrylamide): Experiment, theory and application. *Prog. Polym. Sci.* **1992**, *17*, 163–249. [[CrossRef](#)]
157. Hauser, A.W.; Evans, A.A.; Na, J.H.; Hayward, R.C. Photothermally reprogrammable buckling of nanocomposite gel sheets. *Angew. Chem.-Int. Ed.* **2015**, *54*, 5434–5437. [[CrossRef](#)] [[PubMed](#)]
158. Miranda, B.; Moretta, R.; De Martino, S.; Dardano, P.; Rea, I.; Forestiere, C.; De Stefano, L. A PEGDA hydrogel nanocomposite to improve gold nanoparticles stability for novel plasmonic sensing platforms. *J. Appl. Phys.* **2021**, *129*, 033101. [[CrossRef](#)]
159. Lee, S.; Pérez-Luna, V.H. Surface-grafted hybrid material consisting of gold nanoparticles and dextran exhibits mobility and reversible aggregation on a surface. *Langmuir* **2007**, *23*, 5097–5099. [[CrossRef](#)]
160. Gupta, S.; Uhlmann, P.; Agrawal, M.; Chapuis, S.; Oertel, U.; Stamm, M. Immobilization of silver nanoparticles on responsive polymer brushes. *Macromolecules* **2008**, *41*, 2874–2879. [[CrossRef](#)]
161. Ansah, I.B.; Kim, S.; Yang, J.-Y.; Mun, C.; Jung, H.S.; Lee, S.; Kim, D.-H.; Kim, S.-H.; Park, S.-G.; Ansah, I.B.; et al. In Situ Electrodeposition of Gold Nanostructures in 3D Ultra-Thin Hydrogel Skins for Direct Molecular Detection in Complex Mixtures with High Sensitivity. *Laser Photon. Rev.* **2021**, *15*, 2100316. [[CrossRef](#)]
162. Conde, J.; Dias, J.T.; Grazú, V.; Moros, M.; Baptista, P.V.; de la Fuente, J.M. Revisiting 30 years of biofunctionalization and surface chemistry of inorganic nanoparticles for nanomedicine. *Front. Chem.* **2014**, *2*, 48. [[CrossRef](#)]
163. Politi, J.; Spadavecchia, J.; Fiorentino, G.; Antonucci, I.; De Stefano, L. Arsenate reductase from *Thermus thermophilus* conjugated to polyethylene glycol-stabilized gold nanospheres allow trace sensing and speciation of arsenic ions. *J. R. Soc. Interface* **2016**, *13*, 20160629. [[CrossRef](#)]
164. Wang, S.; Wang, A.; Ma, Y.; Han, Q.; Chen, Y.; Li, X.; Wu, S.; Li, J.; Bai, S.; Yin, J. In situ synthesis of superorganism-like Au NPs within microgels with ultra-wide absorption in visible and near-infrared regions for combined cancer therapy. *Biomater. Sci.* **2021**, *9*, 774–779. [[CrossRef](#)] [[PubMed](#)]
165. Endo, T.; Ikeda, R.; Yanagida, Y.; Hatsuzawa, T. Stimuli-responsive hydrogel-silver nanoparticles composite for development of localized surface plasmon resonance-based optical biosensor. *Anal. Chim. Acta* **2008**, *611*, 205–211. [[CrossRef](#)] [[PubMed](#)]
166. Joshi, G.K.; Deitz-Mcelyea, S.; Johnson, M.; Mali, S.; Korc, M.; Sardar, R. Highly specific plasmonic biosensors for ultrasensitive MicroRNA detection in plasma from pancreatic cancer patients. *Nano Lett.* **2014**, *14*, 6955–6963. [[CrossRef](#)] [[PubMed](#)]
167. Huang, C.; Bonroy, K.; Reekmans, G.; Laureyn, W.; Verhaegen, K.; De Vlamincq, I.; Lagae, L.; Borghs, G. Localized surface plasmon resonance biosensor integrated with microfluidic chip. *Biomed. Microdevices* **2009**, *11*, 893–901. [[CrossRef](#)]
168. Rebelo, R.; Barbosa, A.I.; Caballero, D.; Kwon, I.K.; Oliveira, J.M.; Kundu, S.C.; Reis, R.L.; Correló, V.M. 3D biosensors in advanced medical diagnostics of high mortality diseases. *Biosens. Bioelectron.* **2019**, *130*, 20–39. [[CrossRef](#)]
169. Randriantsilefisoa, R.; Nie, C.; Parshad, B.; Pan, Y.; Bhatia, S.; Haag, R. Double trouble for viruses: A hydrogel nanocomposite catches the influenza virus while shrinking and changing color. *Chem. Commun.* **2020**, *56*, 3547–3550. [[CrossRef](#)]
170. Abalde-Cela, S.; Augui, B.; Fischlechner, M.; S Huck, W.T.; Alvarez-Puebla, R.A.; Liz-Marzán, L.M.; Abell, C. Microdroplet fabrication of silver-agarose nanocomposite beads for SERS optical accumulation. *Soft Matter* **2011**, *7*, 1321–1325. [[CrossRef](#)]
171. Aldeanueva-Potel, P.; Faucher, E.; Alvarez-Puebla, R.A.; Liz-Marzán, L.M.; Brust, M. Recyclable Molecular Trapping and SERS Detection in Silver-Loaded Agarose Gels with Dynamic Hot Spots. *Anal. Chem.* **2009**, *81*, 9233–9238. [[CrossRef](#)]
172. Bodelón, G.; Montes-García, V.; López-Puente, V.; Hill, E.H.; Hamon, C.; Sanz-Ortiz, M.N.; Rodal-Cedeira, S.; Costas, C.; Celiksoy, S.; Pérez-Juste, I.; et al. Detection and imaging of quorum sensing in *Pseudomonas aeruginosa* biofilm communities by surface-enhanced resonance Raman scattering. *Nat. Mater.* **2016**, *15*, 1203–1211. [[CrossRef](#)]
173. Ham, J.; Yun, B.J.; Koh, W.G. SERS-based biosensing platform using shape-coded hydrogel microparticles incorporating silver nanoparticles. *Sens. Actuators B Chem.* **2021**, *341*, 129989. [[CrossRef](#)]
174. Liu, Y.; Zhang, X. Microfluidics-Based Plasmonic Biosensing System Based on Patterned Plasmonic Nanostructure Arrays. *Micromachines* **2021**, *12*, 826. [[CrossRef](#)] [[PubMed](#)]
175. Homola, J. Present and future of surface plasmon resonance biosensors. *Anal. Bioanal. Chem.* **2003**, *377*, 528–539. [[CrossRef](#)]
176. Cooper, M.A. Optical biosensors in drug discovery. *Nat. Rev. Drug Discov.* **2002**, *1*, 515–528. [[CrossRef](#)]
177. Wang, Y.; Zhou, J.; Li, J. Construction of Plasmonic Nano-Biosensor-Based Devices for Point-of-Care Testing. *Small Methods* **2017**, *1*, 1700197. [[CrossRef](#)]
178. Tu, J.; Torrente-Rodríguez, R.M.; Wang, M.; Gao, W. The Era of Digital Health: A Review of Portable and Wearable Affinity Biosensors. *Adv. Funct. Mater.* **2020**, *30*, 1906713. [[CrossRef](#)]
179. Kumar, S.; Kumar, S.; Ali, M.A.; Anand, P.; Agrawal, V.V.; John, R.; Maji, S.; Malhotra, B.D. Microfluidic-integrated biosensors: Prospects for point-of-care diagnostics. *Biotechnol. J.* **2013**, *8*, 1267–1279. [[CrossRef](#)]
180. Nikoleli, G.P.; Siontorou, C.G.; Nikolelis, D.P.; Bratakou, S.; Karapetis, S.; Tzamtzis, N. Biosensors Based on Microfluidic Devices Lab-on-a-Chip and Microfluidic Technology. *Nanotechnol. Biosens.* **2018**, *6*, 375–394. [[CrossRef](#)]
181. Borghei, Y.S.; Hosseinkhani, S.; Ganjali, M.R. “Plasmonic Nanomaterials”: An emerging avenue in biomedical and biomedical engineering opportunities. *J. Adv. Res.* **2021**; *in press*. [[CrossRef](#)]
182. Liu, J.; Jalali, M.; Mahshid, S.; Wachsmann-Hogiu, S. Are plasmonic optical biosensors ready for use in point-of-need applications? *Analyst* **2020**, *145*, 364–384. [[CrossRef](#)]
183. Liao, Z.; Zhang, Y.; Li, Y.; Miao, Y.; Gao, S.; Lin, F.; Deng, Y.; Geng, L. Microfluidic chip coupled with optical biosensors for simultaneous detection of multiple analytes: A review. *Biosens. Bioelectron.* **2019**, *126*, 697–706. [[CrossRef](#)]
184. Geng, Z.; Zhang, X.; Fan, Z.; Lv, X.; Su, Y.; Chen, H. Recent Progress in Optical Biosensors Based on Smartphone Platforms. *Sensors* **2017**, *17*, 2449. [[CrossRef](#)] [[PubMed](#)]

185. Liu, Y.; Zhang, N.; Li, P.; Yu, L.; Chen, S.; Zhang, Y.; Jing, Z.; Peng, W. Low-cost localized surface plasmon resonance biosensing platform with a response enhancement for protein detection. *Nanomaterials* **2019**, *9*, 1019. [[CrossRef](#)] [[PubMed](#)]
186. Chen, P.; Chung, M.T.; McHugh, W.; Nidetz, R.; Li, Y.; Fu, J.; Cornell, T.T.; Shanley, T.P.; Kurabayashi, K. Multiplex serum cytokine immunoassay using nanoplasmonic biosensor microarrays. *ACS Nano* **2015**, *9*, 4173–4181. [[CrossRef](#)] [[PubMed](#)]
187. Cappi, G.; Spiga, F.M.; Moncada, Y.; Ferretti, A.; Beyeler, M.; Bianchessi, M.; Decosterd, L.; Buclin, T.; Guiducci, C. Label-Free detection of tobramycin in serum by transmission-localized surface plasmon resonance. *Anal. Chem.* **2015**, *87*, 5278–5285. [[CrossRef](#)]
188. Cappi, G.; Accastelli, E.; Cantale, V.; Rampi, M.A.; Benini, L.; Guiducci, C. Peak shift measurement of localized surface plasmon resonance by a portable electronic system. *Sens. Actuators B Chem.* **2013**, *176*, 225–231. [[CrossRef](#)]
189. Cantale, V.; Simeone, F.C.; Gambari, R.; Rampi, M.A. Gold nano-islands on FTO as plasmonic nanostructures for biosensors. *Sens. Actuators B Chem.* **2011**, *152*, 206–213. [[CrossRef](#)]
190. Zhou, X.; Wong, T.I.; Song, H.Y.; Wu, L.; Wang, Y.; Bai, P.; Kim, D.H.; Ng, S.H.; Tse, M.S.; Knoll, W. Development of Localized Surface Plasmon Resonance-Based Point-of-Care System. *Plasmonics* **2014**, *9*, 835–844. [[CrossRef](#)]
191. Kim, S.C.; Jalal, U.M.; Im, S.B.; Ko, S.; Shim, J.S. A smartphone-based optical platform for colorimetric analysis of microfluidic device. *Sens. Actuators B Chem.* **2017**, *239*, 52–59. [[CrossRef](#)]
192. Wong, T.I.; Han, S.; Wu, L.; Wang, Y.; Deng, J.; Tan, C.Y.L.; Bai, P.; Loke, Y.C.; Da Yang, X.; Tse, M.S.; et al. High throughput and high yield nanofabrication of precisely designed gold nanohole arrays for fluorescence enhanced detection of biomarkers. *Lab Chip* **2013**, *13*, 2405–2413. [[CrossRef](#)]
193. Minopoli, A.; Acunzo, A.; Della Ventura, B.; Velotta, R. Nanostructured Surfaces as Plasmonic Biosensors: A Review. *Adv. Mater. Interfaces* **2021**, 2101133. [[CrossRef](#)]